2009-08-13

Scan-Based Near-Field Acoustical Holography on Partially Correlated Sources

Michael D. Gardner
Brigham Young University - Provo

SCAN-BASED NEAR-FIELD ACOUSTICAL HOLOGRAPHY ON PARTIALLY CORRELATED SOURCES

by

Michael D. Gardner

A thesis submitted to the faculty of

Brigham Young University

in partial fulfillment of the requirements for the degree of

Master of Science

Department of Physics and Astronomy

Brigham Young University

December 2009

BRIGHAM YOUNG UNIVERSITY

GRADUATE COMMITTEE APPROVAL

of a thesis submitted by

Michael D. Gardner

This thesis has been read by each member of the following graduate committee and by majority vote has been found to be satisfactory.

_____	_____
Date	Kent L. Gee, Chair
_____	_____
Date	Scott D. Sommerfeldt
_____	_____
Date	Jonathan D. Blotter

BRIGHAM YOUNG UNIVERSITY

As chair of the candidate's graduate committee, I have read the thesis of Michael D. Gardner in its final form and have found that (1) its format, citations, and bibliographical style are consistent and acceptable and fulfill university and department style requirements; (2) its illustrative materials including figures, tables, and charts are in place; and (3) the final manuscript is satisfactory to the graduate committee and is ready for submission to the university library.

_____ _____

Date

Kent L. Gee
Chair, Graduate Committee

Accepted for the Department

_____

Ross L. Spencer
Chair, Department of Physics and Astronomy

Accepted for the College

_____

Thomas W. Sederberg
Associate Dean, College of Physical and Mathematical Sciences

ABSTRACT

SCAN-BASED NEAR-FIELD ACOUSTICAL HOLOGRAPHY ON PARTIALLY CORRELATED SOURCES

Michael D. Gardner

Department of Physics and Astronomy

Master of Science

Scan-based near-field acoustical holography (NAH) is applied to partially correlated sources. Partial field decomposition via the virtual coherence method is used to implement the scan-based NAH. The background and theory of these methods are developed. Multiple stationary reference microphones are required for the partial field decomposition. Guidelines for reference microphone placement in the literature thus far have been limited. Improved guidelines for reference microphones are given after the results of two sets of experiments. The first set involves discrete, partially correlated sources, both physical and numerical. The second set of experiments is strictly numerical and involves continuous sources. Fewer microphones are required for partially correlated sources as compared to completely uncorrelated sources. Reference microphone number is found to be more critical to reducing holography reconstruction errors than is placement or location. For the continuous results, an appropriate figure of merit is

created: reference microphones per coherence length. Based upon the definition of coherence length, two reference microphones per coherence length are required to minimize reconstruction error. Further practical reference microphone guidelines are given. These guidelines are to assist in preparing for a full-scale application of scan-based near-field acoustical holography to a military aircraft jet.

ACKNOWLEDGMENTS

I would like to thank Blue Ridge Research and Consulting in conjunction with the Air Force Research Laboratory as well as the Brigham Young University Department of Physics and Astronomy for funding me. I thank Dr. Gee, Alan Wall, Daniel Manwill, Dr. Sommerfeldt, and Dr. Blotter for collaborating and assisting me in the research. I thank my wife for encouraging me to finish.

TABLE OF CONTENTS

LIST OF TABLES

LIST OF FIGURES

CHAPTER 1

INTRODUCTION

This thesis treats the use of scan-based near-field acoustical holography (NAH) on partially correlated sources. The particular project goal is to investigate NAH as a method to better characterize full-scale military jet noise sources. There are two main chapters discussing the research results. They are each slightly modified manuscripts intended to be submitted to peer-reviewed journals. Therefore, each chapter has its own introduction and conclusion, with the chapters reviewing a bit of the same material and using many of the same references.

Chapter 2 describes experiments using scan-based NAH on discrete, partially correlated sources. The topic is introduced and then the methods are explained. These method explanations include an overview of NAH and a detailed development of the partial field decomposition method via virtual coherence (a method necessary when using scan-based NAH on sources which are not coherent). The experiment specifics are explained and results and conclusions are given.

Chapter 3 extends the results of Chapter 2 to continuous sources. Immediately after the introduction, the experiment is discussed. The experimental background is given and a new figure of merit (reference microphones per coherence length) that has been created is explained. Incorporation of the effect of spatial variation of source amplitude on reconstruction error is explained with relevant results discussed. A case study is performed which investigates window-like effects on reference microphone

placement. The chapter also discusses reference microphone guidelines with practical implementation in mind. The issues of coherence, block size, and propagation delay are discussed briefly and conclusions are given. An appendix is given showing the virtual coherence and SONAH codes (with dependent sub-functions) generated in MATLAB®.

CHAPTER 2

SCAN-BASED NEAR-FIELD ACOUSTICAL HOLOGRAPHY ON DISCRETE, PARTIALLY CORRELATED SOURCES

2.1 Introduction

The characterization of the noise source region in high-powered jet engine exhaust is needed to create better noise prediction models and noise reduction schemes.[1,2] Theoretical and semi-empirical models have been used to study jet noise sources,[3,4] while experimental investigations have frequently been used to verify far-field predictions of theoretical models.[5-8] One experimental technique, beamforming, is an array-based method used to characterize jet noise. It is typically performed in the far-field and can give source amplitudes and directivities of jets, especially at high frequencies.[9] Beamforming and other array-techniques such as the acoustic mirror, acoustic telescope, and the polar-correlation technique are limited in resolution and rely on assumptions that the jet noise is emanating from uncorrelated, simple sources.[9]

Near-field acoustical holography (NAH) is a method which has only recently been used on aeroacoustic sources and is the focus of this paper.[10,11] NAH potentially offers greater, more detailed information about noise sources than other array-based methods such as beamforming, especially at low frequencies.[9] Although primarily used in correlated radiation from vibrating structures, NAH may also be used on partially correlated sources, like the noise-generating turbulence in jets.[12] The terms coherent and correlated will be used interchangeably in this thesis; even though, for acoustic signals,

coherence is done in frequency and correlation is done in time, the two are related and both are measures of the linear relationship between signals.

This chapter does not directly address the use of NAH to characterize jet noise, but rather treats a critical part of the overall problem. In particular, the number and placement of reference microphones (required for scan-based NAH) will be investigated through physical and numerical experiments on partially correlated sources. In order to better understand guidelines for reference microphone placement and number, the physical experiments will be carried out with controlled, partially correlated sources. The remainder of this chapter will develop the virtual coherence method (which allows one to perform scan-based NAH on fields which are not fully coherent), explain the physical and numerical experiments, give their results, and issue conclusions

2.2 Methods

2.2.1 Scan-based near-field acoustical holography

Near-field acoustical holography relies on Green's functions that are solutions to the Helmholtz equation. Acoustic pressure measurements are made on a surface (hologram) in the near field of a source, and the Green's functions are then used to propagate the field back to the source surface (or elsewhere).[13] Reconstructions of acoustic pressure, particle velocity, and acoustic intensity can be made in the entire three-dimensional region outside the source region. One constraint of an NAH measurement is that it requires a coherent acoustic field in order to make proper reconstructions. A coherent field means there is a constant phase relationship between every pair of points in the field. If the measurement is made at all points simultaneously ("snap-shot" approach), the

coherence requirement is met. Even in a simultaneous measurement, the coherence requirement is only met if a single Fourier transform of a time block is performed; no averaging can be done without a reference signal. Additionally, simultaneous measurements are often impractical when a large number of measurement points (and thus microphones) is required.

There are several NAH methods. Statistically optimized near-field acoustical holography (SONAH) is the specific method of NAH that is used here. The theory of SONAH will not be given here but is given in other articles.[14-17] In brief, SONAH is a wave-function-expansion-based method of NAH (as opposed to a Fourier-transform-based approach) which also allows greater freedom in measurement points compared to other methods and the experiments herein make use of SONAH in Cartesian coordinates. A few parameters in the SONAH processing that can be adjusted to optimize a particular measurement are the maximum wave numbers, k_y and k_z, to include in several of the matrices in SONAH, the grid spacing of the k_y and k_z wave vectors in this matrices, i.e. Δk_y and Δk_z, and the regularization parameter. There are optimal values given in the literature for Δk_y, Δk_z, maximum k_y, and maximum k_z.[17] However, minor tuning of these parameters can still yield more optimal results. Ideally, k_y and k_z extend to infinity as Δk_y and Δk_z tend towards zero. The necessary mathematical formulation has been determined for these ideal limits for the parameter values;[17] however, it involves performing many computationally expensive numerical integrals, and was therefore not included in this application of SONAH. The maximum k_y and k_z values set equal to $2\pi/\Delta y$ and $2\pi/\Delta z$, respectively, where Δy and Δz are the spacing between grid points in those directions. Δk_y and Δk_z were set equal to $\pi/2L_y$ and $\pi/2L_z$, respectively, where L_y and L_z were the

lengths of the grid in those two directions. These values were used throughout this thesis and were never changed. The choice of regularization parameter was automated via the generalized cross validation (GCV) and the regularization method was modified Tikhonov regularization.[18] Finally, the wave function amplitudes were weighted as per Ref. 17.

Scan-based NAH measurements are performed in situations where the number of desired measurement positions exceeds the number of available microphones. The microphone grid is scanned or moved from position to position across the entire measurement grid, remaining stationary at each scan position to record signals.. With scan-based NAH, the coherence requirement is met via the use of a reference signal to align the phase across multiple scans. Only one reference signal is needed to apply scan-based NAH to vibrating solid structures (the usual subject of NAH investigations, e.g., see Ref. 19) because vibrating structures are usually very coherent. When the field is not fully coherent, as in the case of aeroacoustic sources such as jets,[12] multiple reference signals are required. For clarification, aeroacoustic sources are those which are generated via turbulence in a fluid or the interaction between aerodynamic forces and structures. In fact, aeroacoustic sources have only recently been investigated with NAH.[10] The application of scan-based NAH with multiple reference signals is called partial field decomposition, and partial field decomposition in conjunction with the virtual coherence method will be explained in this thesis. Throughout the thesis, the terms "partial field decomposition" and "virtual coherence method" will be used interchangeably, even though the virtual coherence is only one specific way of performing partial field

decomposition. This is done because only the virtual coherence method was used in this research.

2.2.2 Virtual coherence

2.2.2.1 Background

Hald[20] laid the foundation for the use of partial field decomposition with NAH, outlining the method with an intended application to motor vehicle noise. The method is based upon the broader technique of principal component analysis,[21] wherein a set of random variables with a given variance spread out over the variables, is transformed into a new set of variables where that same variance is mostly contained in the first few variables (principal components). In NAH, the reference signals or variables are transformed into virtual reference signals or variables with the variance ideally concentrated in the first few virtual references. This is akin to identifying and separating the source-related components of the field from the noise-related components. Several have compared a partial coherence method (Gaussian-elimination based) to the virtual coherence method (singular-value-decomposition based).[22,23] The partial coherence method allows partial fields to be generated which have more geometric meaning, whereas the partial fields in the virtual coherence technique lose geometric significance due to the automatic reordering of singular values in the singular value decomposition (SVD). Also, to gain the geometric insight, a reference signal coherent to each subsource is needed. This is a requirement that is difficult to meet for jet noise. Both the partial coherence and virtual coherence methods give similar composite results in ideal situations, although off-diagonal terms in the reference cross-spectral matrix in the partial coherence method can

degrade the partial fields. The virtual coherence method results in a virtual reference cross-spectral matrix which is diagonal and therefore no off-diagonal terms to degrade partial fields.

Nam and Kim[24-25] laid out a method (similar in effect to the partial coherence method) to determine each individual sound field generated by each incoherent source by assuming the separate fields from each of the sources hardly overlap on the source plane. This, however, requires *a priori* knowledge of the number of incoherent sources and that the sources be incoherent. Although this latter assumption is identical to that made by phased-array beamforming methods, it loses applicability in jet noise because of the distributed, extended, and partially-correlated nature of the source.

Others have improved upon the theory of virtual coherence. Kwon *et al.*[26] and Lee and Bolton[27] outline the necessary modifications of partial field decomposition to account for source-level variation or source nonstationarity from scan to scan. The method has been applied to pass-by-noise tests by incorporating time-dependence into the processing.[28] Scan-based NAH was applied to aeroacoustic sources including a fan and a small subsonic jet by Lee and Bolton.[10,11] NAH tests (not scan-based) were performed on subscale jets by Long *et al.*[29] and showed their results agree with conventional beamforming results for jet noise source distribution. This latest application of virtual coherence to a jet most closely mimics the current objective, although the current project will be applied to a full-scale, potentially supersonic jet and the NAH performed will be scan-based.

The virtual coherence method permits scan-based near-field acoustical holography without restrictions on coherence.[20] This is accomplished through multiple reference microphones which are stationary throughout the scans.

2.2.2.2 Theory

The development of the virtual coherence method follows that of Lee and Bolton[27] and Otte *et al*.[30] This method uses the signals at the reference microphones to decompose the incoherent sound field into coherent partial fields that are mutually incoherent. Because each of these partial fields meets the coherence requirement for holography, SONAH or another NAH method can be used to reconstruct an individual partial field elsewhere. However, because the partial fields are mutually incoherent, the reconstructed partial fields are added on an intensity basis to obtain a resultant field.

Assume that there is some matrix, $\mathbf{H}_{rp}$, which is the transfer function from the reference microphones to the measurement points for each scan, such that

$$\mathbf{p} = \mathbf{H}_{rp}^{T}\,\mathbf{r}, \tag{2.1}$$

where $\mathbf{p} = \begin{bmatrix} p_{11} & \cdots & p_{1N} \\ \vdots & \ddots & \vdots \\ p_{T1} & \cdots & p_{TN} \end{bmatrix}^{\mathrm{T}}$, and $\mathbf{r} = \begin{bmatrix} r_{11} & \cdots & r_{1M} \\ \vdots & \ddots & \vdots \\ r_{T1} & \cdots & r_{TM} \end{bmatrix}^{\mathrm{T}}$. In Eq. 2.1, N is the number of measurement points across one scan, T is the number of acquired time blocks per scan, M is the number of references, and $^{\mathrm{T}}$ represents the transpose operator.[24,30] The matrices $\mathbf{p}$ and $\mathbf{r}$ represent the complex amplitude of the pressure at one frequency (assuming $e^{j\omega t}$ time dependence) at the measurement points and reference points, respectively. In the limit as $T \to \infty$, the cross-spectral matrices become true expectation value matrices. The cross-spectral matrices $\boldsymbol{C}_{rr}$, $\boldsymbol{C}_{rp}$, and $\mathbf{C}_{pp}$ are defined as

$$\mathbf{C}_{rr} = \mathbf{r}^{*}\mathbf{r}^{\mathrm{T}} , \tag{2.2}$$

$$\mathbf{C}_{rp} = \mathbf{r}^{*}\mathbf{p}^{\mathrm{T}}, \tag{2.3}$$

and

$$\mathbf{C}_{pp} = \mathbf{p}^{*}\mathbf{p}^{\mathrm{T}}, \tag{2.4}$$

where * represents the complex conjugate. The transfer equation in Eq. 2.1 can now be represented as

$$\mathbf{H}_{rp} = \mathbf{C}_{rr}^{-1}\mathbf{C}_{rp} . \tag{2.5}$$

Because the cross-spectral matrix $\mathbf{C}_{rr}$ will generally have a high condition number,it is not well-suited for inversion. The high condition number is present because the reference microphones will inevitably be contaminated by noise. The virtual coherence method converts the actual reference cross-spectral matrix into a diagonal virtual reference cross-spectral matrix, via the SVD as shown in Eq. 2.6.

$$\mathbf{C}_{rr} = \mathbf{U}\mathbf{\Sigma}\mathbf{V}^{\mathrm{H}} = \mathbf{U}\mathbf{\Sigma}\mathbf{U}^{\mathrm{H}} , \tag{2.6}$$

where **U** and **V** are left and right unitary matrices containing the left and right singular vectors of $\mathbf{C}_{rr}$ and $\mathbf{\Sigma}$ is the diagonal matrix of singular values. The superscript $^{\mathrm{H}}$ represents the Hermitian transpose. **U** and **V** are equal in this case because $\mathbf{C}_{rr}$ is positive semi-definite and Hermitian. It is semi-definite because all the diagonal elements (auto-spectra) are greater than or equal to zero, and it is Hermitian owing to the symmetry inherent in cross-spectral matrices. Multiplication of matrices in the real reference domain by **U** converts them to the virtual reference domain as

$$\mathbf{\Sigma} = \mathbf{U}^{\mathrm{H}}\mathbf{C}_{rr}\mathbf{U} = \mathbf{v}^{*}\mathbf{v}^{\mathrm{T}} = \mathbf{C}_{vv}\ , \tag{2.7}$$

where $\mathbf{v}$ represents the virtual reference matrix and $\mathbf{C}_{vv}$ represents the virtual reference cross-spectral matrix. Note that the $\mathbf{C}_{vv}$ matrix is diagonal because it is a singular value matrix whereas the $\mathbf{C}_{rr}$ matrix is not. This means the virtual reference signals are completely independent of one another. The transfer matrix from the virtual references to the measurement points is

$$\mathbf{H}_{vp} = \mathbf{\Sigma}^{-1}\mathbf{U}^{\mathrm{H}}\mathbf{C}_{rp}\,. \tag{2.8}$$

The transfer matrix, $\mathbf{H}_{vp}$, can now be used to transfer from the virtual references to obtain the partial fields, $\widehat{\mathbf{P}}$, as

$$\widehat{\mathbf{P}} = \mathbf{H}_{vp}^{\mathrm{T}}\mathbf{\Sigma}^{1/2} = \mathbf{C}_{rp}^{\mathrm{T}}\mathbf{U}^{*}\mathbf{\Sigma}^{-1/2}, \tag{2.9}$$

where each column of $\widehat{\mathbf{P}}$ represents a different partial field. Equation 2.9 represents a cross-spectral matrix-based formulation of partial field decomposition.

It should be noted here that for a realistic measurement, the source level can vary from scan to scan which will adversely affect a cross-spectral matrix across scans. A transfer-matrix-based formulation can account for this variance, which will give correct partial field amplitude and phase information relative to the sources. This is given as

$$\widehat{\mathbf{P}} = \mathbf{H}_{vp}^{\mathrm{T}}\mathbf{\Sigma}^{1/2} = \mathbf{H}_{rp}^{\mathrm{T}}\mathbf{U}^{*}\mathbf{\Sigma}^{1/2}. \tag{2.10}$$

The problem with this formulation is that it requires regularization due to the inversion of the matrix $\mathbf{C}_{rr}$. This is accomplished via a truncated singular value decomposition (TSVD) of $\mathbf{C}_{rr}$.[27] Note that the number of cross-spectral matrices ($\mathbf{C}_{rr}$ and $\boldsymbol{C}_{rp}$) obtained

is equal to the number of scans. Therefore, the reference cross-spectral matrices are averaged to minimize error. The TSVD of $\mathbf{C}_{rr}$ is accomplished as

$$\mathbf{C}_{rr}^{+} = \mathbf{U}\boldsymbol{\Sigma}^{+}\mathbf{U}^{\mathrm{H}}, \tag{2.11}$$

where $\boldsymbol{\Sigma}^{+}$ is the regularized inverse of $\boldsymbol{\Sigma}$. The regularization is performed by setting the noise-related singular values equal to zero after the matrix inversion as

$$\boldsymbol{\Sigma}^{+} = \begin{bmatrix} \boldsymbol{\Sigma}_s & \mathbf{0} \\ \mathbf{0} & \boldsymbol{\Sigma}_n \end{bmatrix}^{+} = \begin{bmatrix} \boldsymbol{\Sigma}_s^{-1} & \mathbf{0} \\ \mathbf{0} & \mathbf{0} \end{bmatrix}, \tag{2.12}$$

where the subscripts *s* and *n* represent source-related and noise-related values respectively. Equation (2.10) is now

$$\begin{aligned} \widehat{\mathbf{P}} &= \left[\mathbf{C}_{rr\,(\mathrm{scan})}^{+}\mathbf{C}_{rp\,(\mathrm{scan})}\right]^{\mathrm{T}}\mathbf{U}_{(\mathrm{avg})}^{*}\boldsymbol{\Sigma}_{(\mathrm{avg})}^{1/2} \\ &= \left[\mathbf{U}_{(\mathrm{scan})}\boldsymbol{\Sigma}_{(\mathrm{scan})}^{+}\mathbf{U}_{(\mathrm{scan})}^{\mathrm{H}}\mathbf{C}_{rp\,(\mathrm{scan})}\right]^{\mathrm{T}}\mathbf{U}_{(\mathrm{avg})}^{*}\boldsymbol{\Sigma}_{(\mathrm{avg})}^{1/2}. \end{aligned} \tag{2.13}$$

Equation 2.13 now accounts for source level variation through the transfer function and it also accounts for statistical measurement noise through averaging. However, Eq. 2.13 does not average out cross-spectral noise as well as Eq. 2.9 does. Therefore, depending on the situation, either Eq. 2.13 or Eq. 2.9 will be more suitable. In this thesis, Eq. 2.13 is used throughout.

When the singular values exhibit a clear, observable drop in amplitude, the choice is obvious that these smaller (noise-related) singular values are to be set to zero in the regularized inverse of $\boldsymbol{\Sigma}$. If the distinction between source- and noise-related singular values is not clear, the virtual coherence function will allow determination of a proper cutoff singular value. The virtual coherence function also allows the determination of the

sufficiency of the reference microphone set. The virtual coherence is the coherence between the virtual references and the field measurement points and is defined as

$$\gamma_{ij}^2 = \frac{\left|\mathbf{C}_{v_j p_i}\right|^2}{\mathbf{C}_{p_i p_i}\mathbf{C}_{v_j v_j}}, \tag{2.14}$$

where the subscripts *i* and *j* denote the *i*th measurement point and the *j*th partial field. The virtual coherence method is so named because of this function. If the sum of this coherence function across the partial fields approaches one for all measurement points (see Eq. 2.15), then the reference set is sufficient.

$$\sum_{j=1}^{\mathrm{R}} \gamma_{ij}^2 \approx 1 \quad for\ i = 1,2,\ldots,N\ . \tag{2.15}$$

R is the number of source-related singular values and partial fields and N is the total number of measurement points. Furthermore, the number of partial fields required to approach one is the number of singular values to keep in the TSVD of $\mathbf{C}_{rr}$.

There needs to be as many reference microphones as there are independent sources, although more are usually required due to noise.[22] Because the sum of the diagonal elements of $\mathbf{C}_{rr}$ is equal to the sum of the elements of $\mathbf{\Sigma}$, having more references allows one to more clearly differentiate the source- and noise-related singular values because the additional energy (from the extra references) will be added to the source-related singular values while the noise-related values will not change.[27]

The partial fields (columns of $\hat{\mathbf{P}}$ in Eqs. 2.9-10 and Eq. 2.13) are then individually processed by NAH (SONAH in this case) and reconstructed at the source surface. With appropriate propagators, NAH can provide pressure, particle velocity, and

intensity (via both pressure and velocity). Pressure or velocity can be added quadratically to obtain magnitude-only total reconstructions as

$$\mathbf{P}_{total} = \sqrt{|\mathbf{P}_1|^2 + |\mathbf{P}_2|^2 + \cdots + |\mathbf{P}_R|^2}, \tag{2.16}$$

where the subscripts 1, 2, and *R* represent the 1st, 2nd, and *R*th reconstructed partial field. Phase information is unavailable across partial fields (due to their mutual incoherence) and thus the partial fields are added quadratically. Finally, total time-averaged intensity reconstructions are possible because the time-averaged intensities for each coherent partial field are added together vectorially.

2.3 Experiment Background

Because jet noise is partially correlated (i.e. there is a finite distance over which the jet field is coherent), experiments have been devised to investigate the effect of partially correlated sources on reference microphone number and placement. Both physical and numerical experiments were performed. For the physical experiment, four loudspeaker sources generated Gaussian noise in an anechoic chamber. The degree of correlation between the four loudspeakers was controlled and varied in four increments: uncorrelated, moderately correlated, highly correlated, and fully correlated. Figure 2-1 shows the correlation coefficient of the four total signals sent to the loudspeakers as a function of correlation condition.[31] There were four independent source signals that were sent in varying amounts to each loudspeaker to obtain the appropriate degree of correlation. If a nonzero degree of correlation was desired, then it was accomplished as follows: Signal 1 was sent to speaker 1 alone; the output for the remaining speakers (from two to four) in relation to the signals is given in this manner:

$$Source_i = \frac{(Source_{i-1} + b \times Signal_i)}{1 + b}, for\ i = 1, 2, \ldots, Q. \tag{2.17}$$

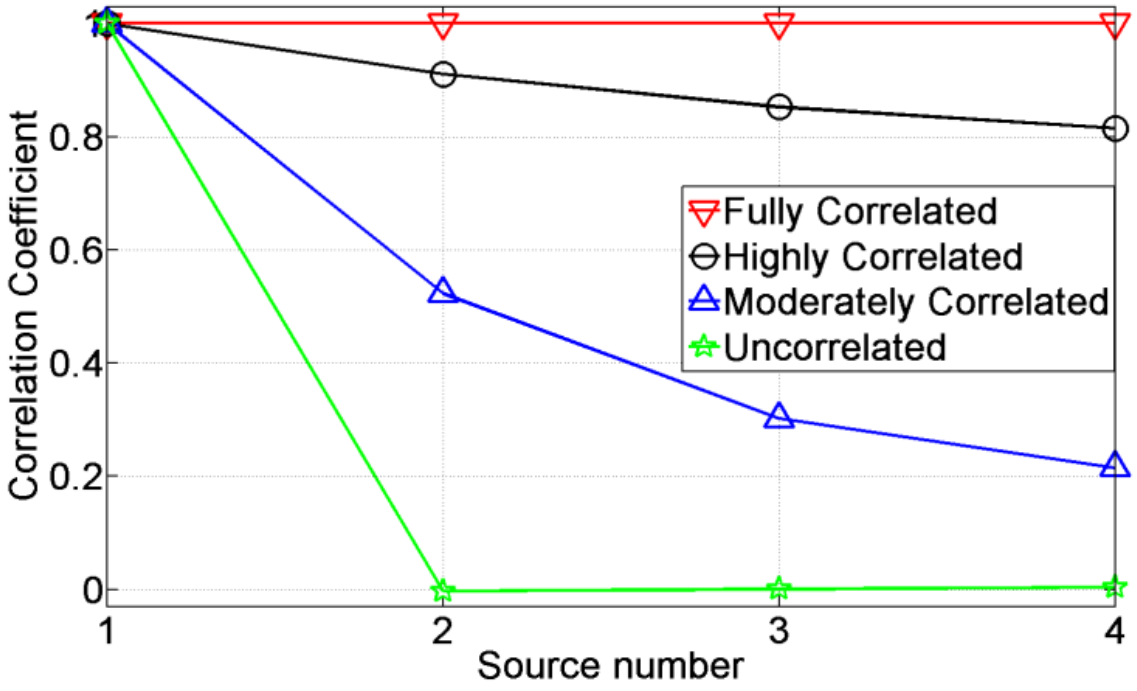

Figure 2-1 Correlation coefficient between the first source and all sources (source nos. 1-4) in the physical experiment for all degrees of correlation.

In Eq. 2.17, *i* is the source number (one to four here), *Q* is the total number of sources (four in this case) and *b* is some factor that determines how correlated the sources will be. The factor *b* equals zero for the fully correlated case, 1.0 for the moderately correlated case, and 0.3 for the highly correlated case sources in this specific case. This method of generating partially correlated sources accounted for the increase in coherence that occurs downstream in a jet[3] (due to the convective turbulence) by including the entire source signal from the previous adjacent source. For the measurement, a vertical array of five

microphones was scanned 473 times to form an 11x43 grid with equal 7.62 cm spacing. There were five horizontal scanning planes for the five microphones in the vertical array spaced at 7.5, 17.5, 27.5, 37.5, and 47.5 cm above the surface of the loudspeakers. The loudspeakers were lined up horizontally at 0 cm (see Fig. 2-2). The 7.5 cm plane was used as a benchmark for reconstructions from higher planes. Results from the 37.5 cm plane will be shown here. Reference microphones were spaced in a horizontal plane two centimeters above the speakers either directly above the sources, in between the sources or in the same relative positions off-axis of the speakers (see Fig. 2-2). Two more were added on the ends. Fig. 2-3 shows a diagram of the measurement points, reconstruction points, sources, and the four references above the sources.

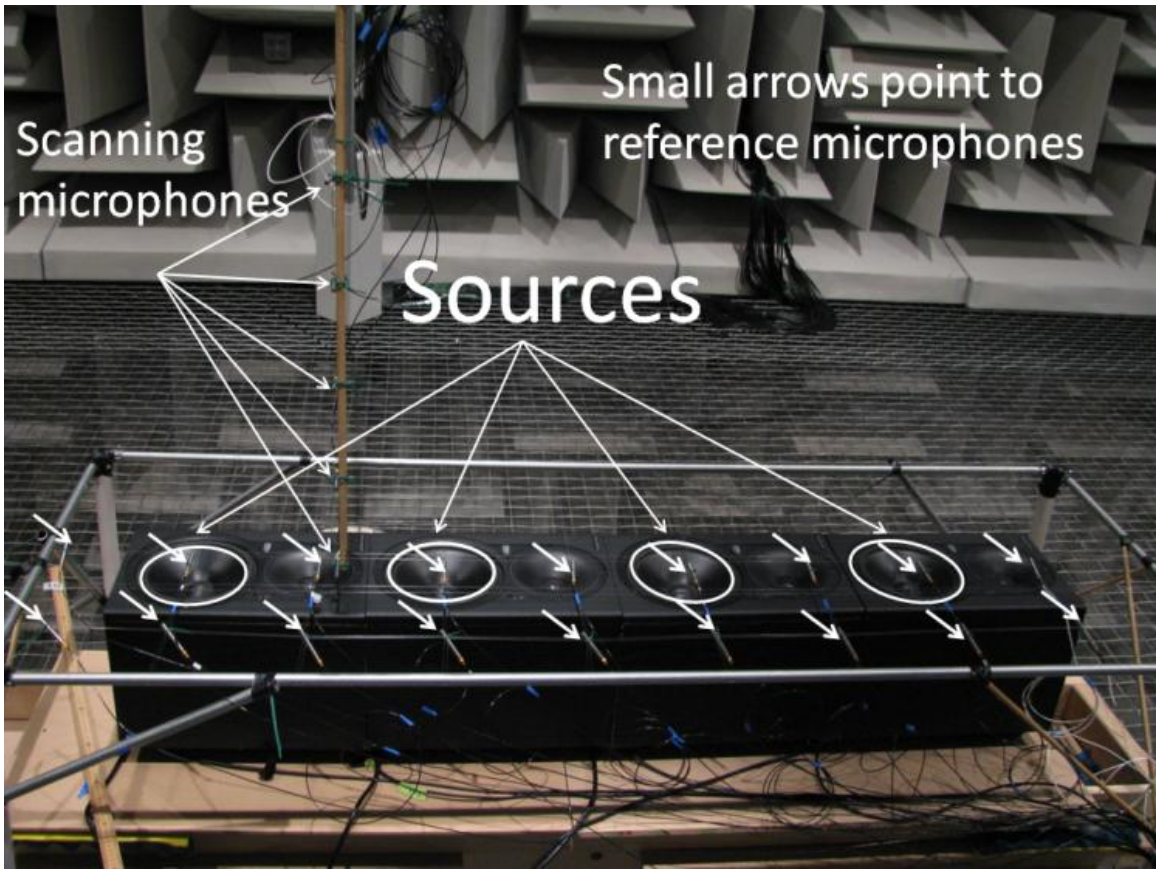

Figure 2-2 Photograph of physical experimental setup showing loudspeaker sources, scanning (measurement) microphones, and reference microphones.

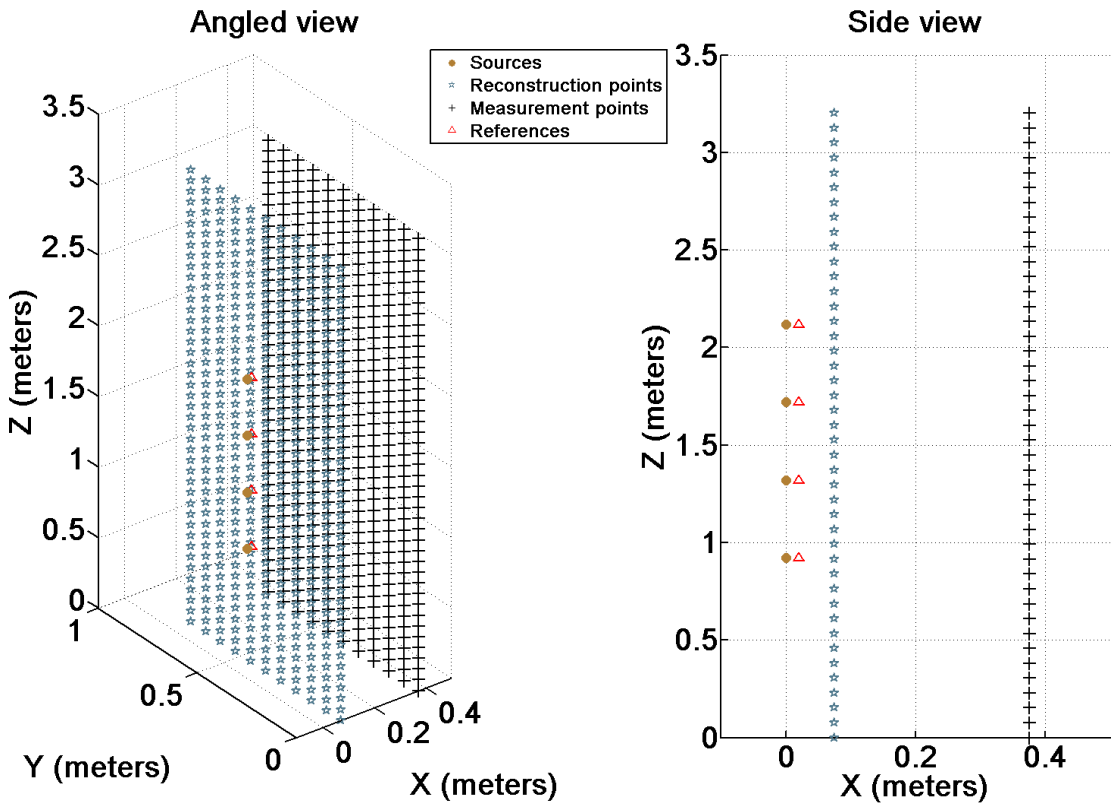

Figure 2-3 Two views of the experiment geometry with the 4 reference microphones above the sources shown as triangles.

The woofers (low-frequency drivers) are considered to be the sources since the frequencies of interest are below the cutoff frequency of the woofers (<1800 Hz). The array was scanned at all positions and the acoustic pressure time waveforms were recorded at the measurement microphones and the reference microphones for all time blocks and scans at a sampling frequency of 50 kHz. Each block had 16,384 samples for a sample time of approximately 0.3277 seconds, and a total of 18 blocks were used per scan. Fourier transforms were performed on the waveforms, converting them to complex pressures (representing one frequency), and then processed by the virtual coherence

method to obtain the partial fields. The partial fields were then processed via SONAH and reconstructed at the horizontal plane 7.5 cm away. Both pressure and velocity were reconstructed so intensities could be calculated as

$$\mathbf{I}_{\chi} = \frac{\mathbf{1}}{\mathbf{2}} \Re\{\mathbf{P}\mathbf{U}_{\chi}^{*}\} \tag{2.18}$$

where the subscript χ means one of the three coordinate directions, **I** denotes the intensity, and **U** denotes the particle velocity.

2.4 Results

2.4.1 Process

An illustration of this process is given in the Figs. 2-4 through 2-6. The measured pressure averaged over blocks at 37.5 cm is shown in Fig. 2-4a for the moderately correlated case. Notice that the field is not smooth and is rather noisy due to the random nature of the sources. The measured data averaged over blocks at the benchmark position is shown in Fig. 2-4b. Because of the uneven nature of the measured data, it was thought that the sum of the partial fields at the benchmark position would constitute a more accurate benchmark (shown in Fig. 2-5c).

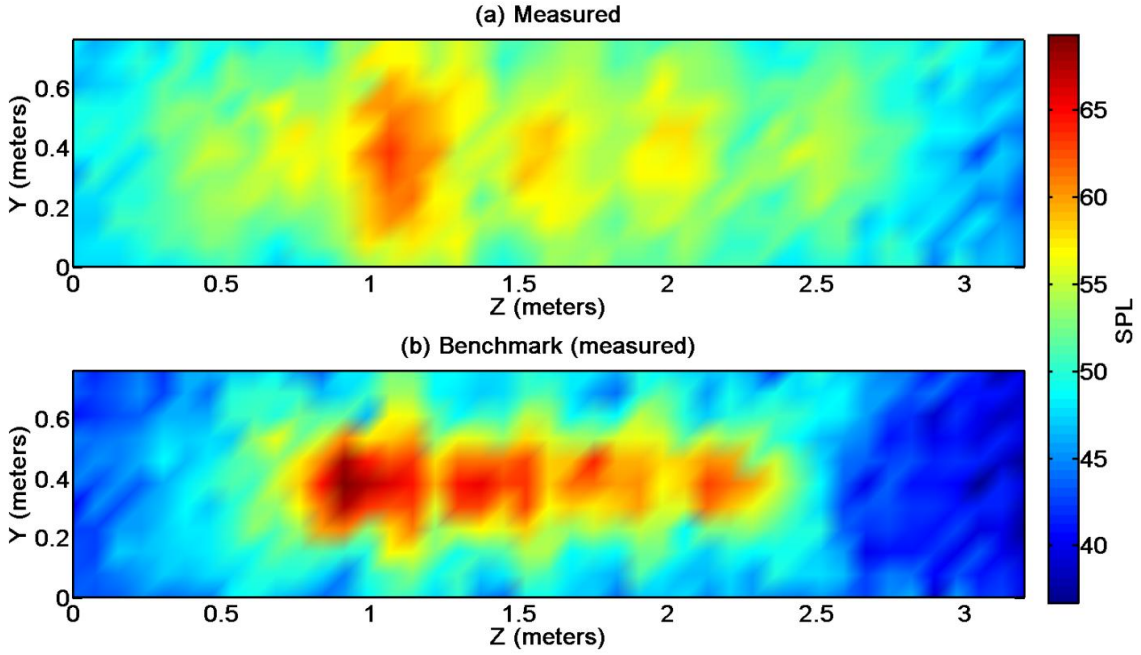

Figure 2-4 Color plots in SPL (dB re 20μPa) of (a) measured data averaged over blocks (18) at 37.5 cm (b) measured data at benchmark position (7.5 cm) averaged over blocks. Both plots are for the moderately correlated case at 900 Hz.

The partial fields themselves are smoother in amplitude and phase than the actual measured fields because of the lack of coherence in the measured field (compare Figs. 2-4 and 2-5). Figure 2-5b shows the reconstructed sound pressure level (dB re 20μPa). The error between the reconstructed and benchmark which was calculated as

$$mean\ error\ (\%) = \sqrt{\frac{\sum_i \left|p_{t,i} - p_{s,i}\right|^2}{\sum_j \left|p_{t,j}\right|^2}} (\times 100), \tag{2.19}$$

where *s* and *t* represent the reconstructed and benchmark pressures, respectively.[27]

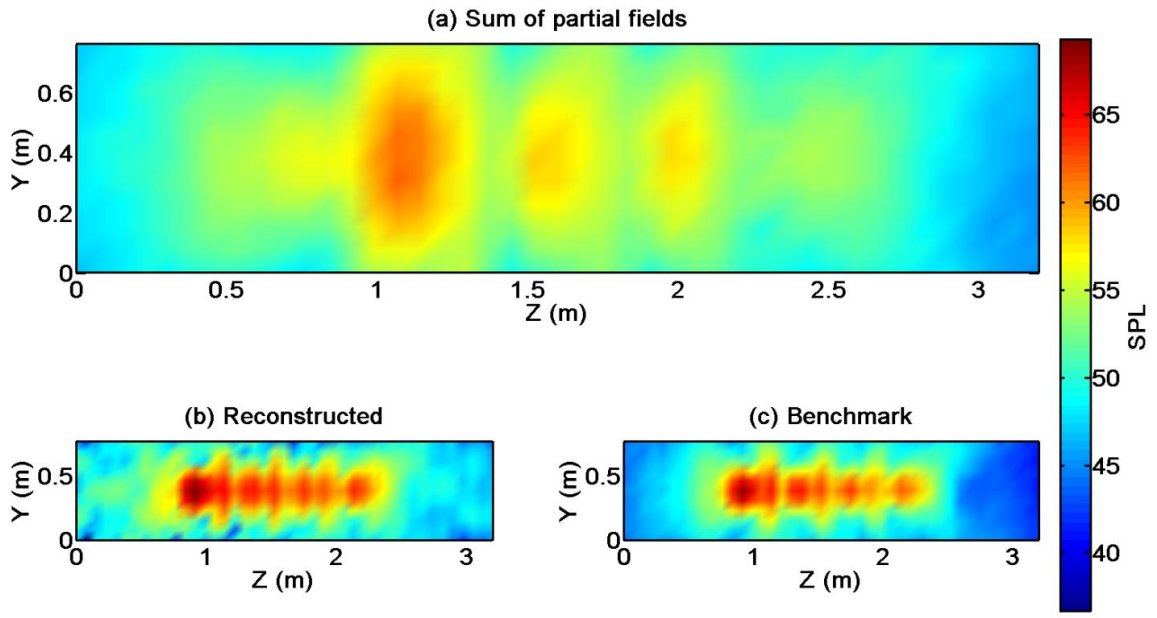

Figure 2-5 Color plots in SPL of (a) measured data averaged over all blocks at 37.5 cm (b) the sum of partial fields at measured at 37.5 cm (c) SONAH reconstructed at 7.5 cm (d) sum of partial fields at benchmark position measured at 7.5 cm All plots are for the moderately correlated case at 900 Hz.

This method of error calculation was chosen because it weights errors more if they occur in higher amplitude regions. Figure 2-5c shows the benchmark SPL 7.5 cm away from the speakers and constitutes the quadratic sum of all the partial fields in that plane. Again, the usage of the partial fields for the benchmark was deemed necessary owing to the scan-based nature of the benchmark measurement. All 18 microphones were used to decompose the partial fields.

The results in Figs. 2-4 and 2-5 are from the moderately correlated case. The more circular high-amplitude regions are directly above the woofers and the correlated nature of the sources shows up with interference regions between the woofers (see Figs. 2-5b and 2-5c). These interference regions do not appear in the uncorrelated case.

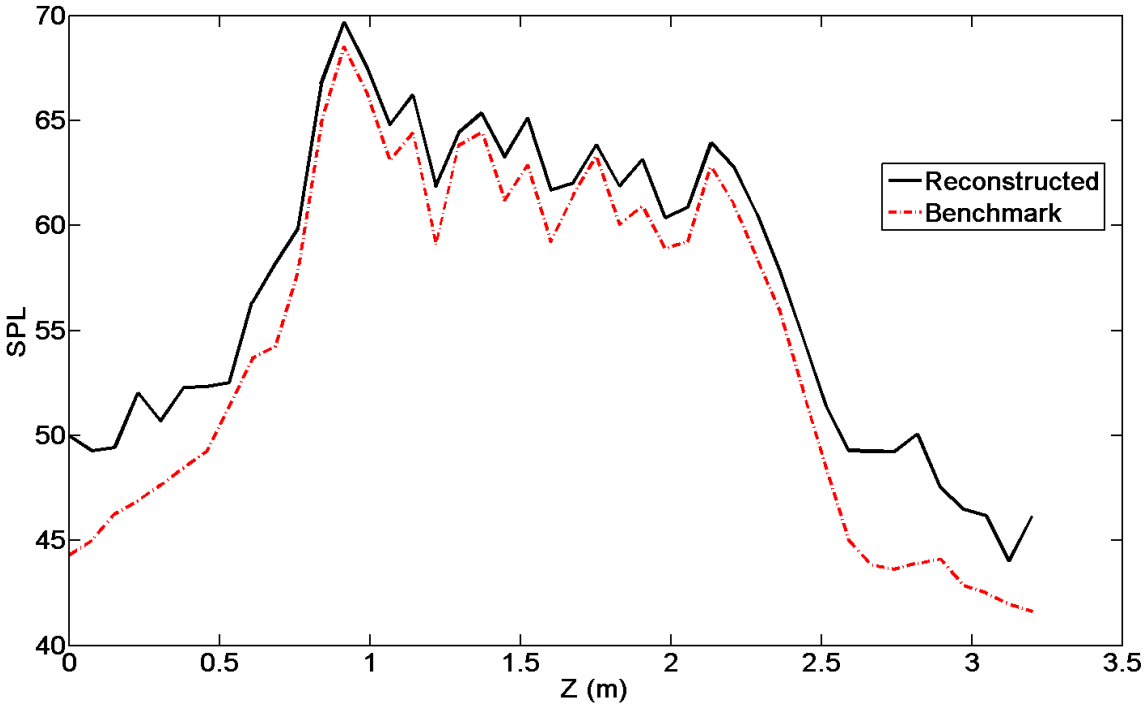

Figure 2-6 Comparison of the reconstructed and benchmarks along a line (parallel to the z-axis) through the center of the pressure map (SPL) at the 7.5 cm plane at 900 Hz for the moderately correlated case.

Figure 2-6 shows SPL for the horizontal line along the z-axis of Figs. 2-5b and 2-5c which is the centerline with respect to the limits of the y-axis. This is also the horizontal line of maximum amplitude and Fig. 2-6 compares the two results with sources and interference regions seen as the peaks in the plot. In addition, most of the error is occurring along the edges (away from the sources) of the window where the overall levels are lower and the reconstruction is overestimating them compared to the benchmark.

The preceding figures have shown magnitude only. However, more information can be obtained if the pressure is combined with the velocity to obtain intensity. Lee and Bolton only showed pressure magnitude plots in their work on the subsonic jet.[11] The

velocity propagator was used in SONAH to get the intensity via Eq. (2.18) and an intensity vector plot superposed with the SPL color map plot is shown in Fig. 2-7 (viewed from an angle to better see the intensity vector directions).[17] As expected, the areas of high intensity are directly above the speaker cones. Note that Fig. 2-7 shows the horizontal plane 7.5 cm above the speakers.

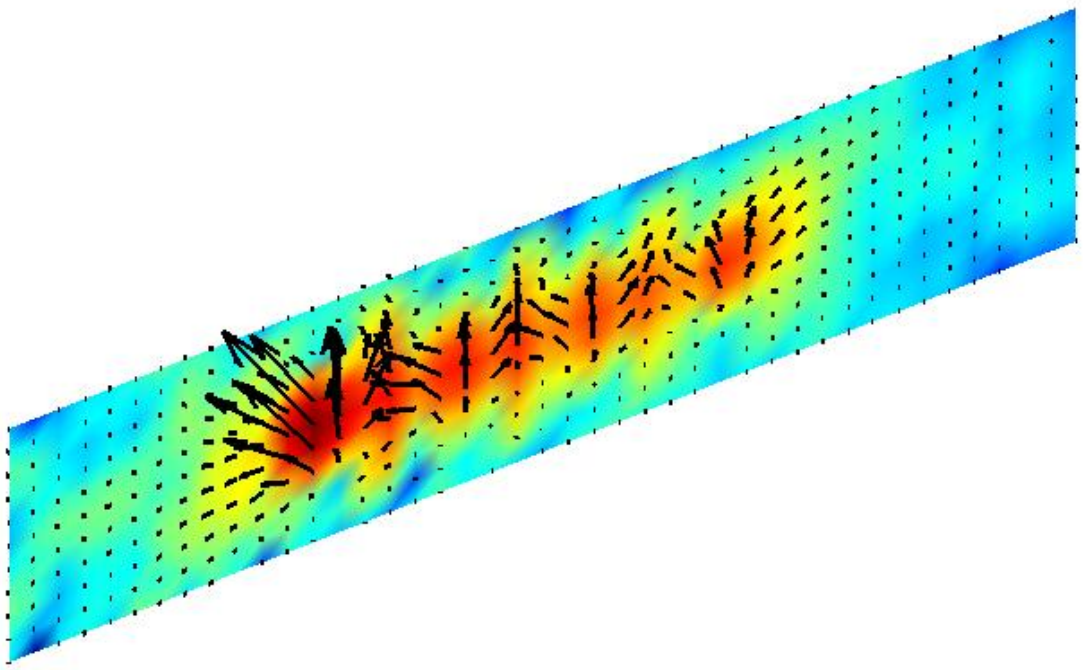

Figure 2-7 Plot showing a superposition of the reconstructed SPL along with 3-component intensity vectors (black) at the same points as the reconstruction. Generated using Eq. (2.18).

2.4.2 Reference microphone number

Enhanced guidelines for reference microphone number are needed where the number of independent sources is unclear. The subsequent results will illustrate the effect of the number of reference microphones on NAH and virtual coherence. The experiment was repeated for different numbers of reference microphones, different degrees of correlation,

and for two frequencies: 300 Hz and 900 Hz. Either one, two, three, four, or all eighteen reference microphones were used; if four or fewer were used, they were located directly above the woofers. The degree of correlation was varied according to Fig. 2-1: fully correlated, highly correlated, moderately correlated, or uncorrelated. These repetitions serve to analyze the effect of reference microphone number and correlation on reconstruction error. The reconstruction error was investigated in addition to mean virtual coherence sum (see Eq. 2.15) This was because a more practical look at the problem was sought, which incorporated the effects of the SONAH processing.

Table 2-1 lists mean percent error and mean virtual coherence sum across partial fields as a function of correlation condition and number of references for two different frequencies (300 Hz and 900 Hz). The SONAH processing was not changed from case to case, although the coherence criterion (see Eq. 2.15) was changed (lowered from 0.999 to 0.95) in certain 18-reference cases in the virtual coherence code to avoid the inclusion of noise-related singular values. The default coherence criterion was 0.999 for all the cases listed in Table 2-1; if the errors were clearly greater (by an order of magnitude or more) than the other cases, the criterion was dropped to 0.95. This is because the virtual coherence code continues to use additional partial fields until the coherence at all the measurement points is greater than or equal to the coherence criterion; therefore, with a coherence criterion which is too high for a given case, it will keep adding partial fields (potentially noise-related) until it has either reached the coherence criterion or exhausted all possible partial fields (the number of reference microphones) This is why in some of the 18-reference cases in Table 2-1, the mean virtual coherence sum is not as high.

Table 2-1 Table of mean errors (in percent) (Eq. 2.19) and mean virtual coherence sum (Eq. 2.15) as a function of number of references, degree of correlation, and frequency (300 and 900 Hz).

Freq	**Refs**	**Fully correlated**		**Highly correlated**		**Moderately correlated**		**Uncorrelated**	
		% error	Mean virtual coherence	% error	Mean virtual coherence	% error	Mean virtual coherence	% error	Mean virtual coherence
300 Hz	18	16.3	0.999	16.9	0.977	32.5	0.982	25.8	0.988
	4	15.1	0.998	17.4	0.995	28.0	0.996	13.7	0.997
	3	15.4	0.997	18.2	0.946	28.2	0.786	31.9	0.784
	2	15.4	0.997	21.3	0.853	48.4	0.539	32.2	0.589
	1	15.1	0.995	33.3	0.790	71.4	0.395	43.6	0.347
900 Hz	18	17.1	0.998	14.5	0.999	25.5	0.999	19.0	0.999
	4	15.8	0.999	16.3	0.998	27.0	0.999	8.17	0.999
	3	16.6	0.999	15.2	0.969	21.5	0.867	42.0	0.766
	2	16.6	0.999	16.9	0.917	27.3	0.670	59.6	0.572
	1	16.4	0.997	20.0	0.811	46.1	0.410	75.2	0.350

Notice that, as expected, only one reference microphone is needed to accurately reconstructed fully coherent sound fields and that there is little variation in the error no matter how many references are used. The theory of principal component analysis predicts this result (i.e. there will be only one principal component for only one source of variation). The general trend (although there are a few exceptions) is that the error increases as fewer reference microphones are used, and this effect is more pronounced

the less correlated the sources are. Notice also the general trend that error increases as coherence decreases.

It was possible to accurately reconstruct the moderately correlated case with only three reference microphones and in the 900 Hz case only two were needed, even though there were four distinct sound radiators with a varying combination of four independent signals. Although this result may seem straightforward since these sources are not completely linearly independent, it was verified and quantified in this controlled physical experiment. It is also significant that an integer reduction in required microphone number is observed (i.e. three microphones as opposed to an unhelpful 3.85 microphones, for example).

In addition, the results with one reference microphone show increasing error with decreasing correlation, showing that the degree of correlation directly affects a one reference NAH measurement. Once the reference microphone count equaled the number of sources, four in this case, increasing beyond this did not reduce the error. There are a few cases where more reference microphones or more correlation actually produce more error. Some of these increases are likely to be statistically insignificant while others can likely be attributed to the fact that the SONAH processing was not optimized (e.g., changing the maximum k_x, maximum k_y, Δk_x, and Δk_y) on a case-by-case basis. In addition, these exceptions generally had the error concentrated away from the source region towards the edges where it is not as crucial. On a final note, the errors may appear to be rather high, e.g., the lowest percentage error in the table is 8.17%. The minimum error is limited by SONAH processing, but the important thing is that once a critical number of reference microphones is reached, the error does not decrease *for that case*.

2.4.3 Reference microphone placement

Focusing attention on location, for this arrangement of microphones, reference microphone placement was not an issue. Table 2-1 shows data when one, two, three, or four references are used and these happen to be directly above the loudspeaker cones. If the location of the one, two, three, or four references is randomized amongst the 18 shown in Fig. 2-2, the results are the same. For example, looking at the four farthest microphones (on the left) form the far right woofer that were not directly above the sources in Fig. 2-2, the mean percent error using these reference microphones for the 900 Hz, moderately correlated case was 22.5%. Compare this to the 27.0% error using the microphones directly above the woofers seen in Table 2-1. Moreover, with these same reference microphones farthest from the far right source in Fig. 2-2, for the 300 Hz, moderately correlated case, the mean error was 28.8% compared to 28.0%. The irrelevance in microphone location in this particular physical experiment likely stems from the fact that the reference microphones were well-separated and well-positioned relative to the sources, i.e., each of the 18 reference microphones could sense all the sources with sufficient fidelity.

Because the physical experiment did not exhibit poor reference microphone placement, a numerical experiment was performed that was similar in every way to the physical experiment except that the loudspeakers were replaced with point sources and the reference microphones could be positioned at any chosen location. When the references were placed in the same places as in the physical experiment, similar trends occurred as in Table 2-1.

Figure 2-8 shows a color plot comparing reconstructions of the physical experiment and the similar numerical experiment. In the plots, only the general shape of the SPL maps can be compared owing to the difference between physical loudspeakers and numerical point sources. However, the circular regions of high amplitude and interference regions appear in similar locations in both cases, suggesting that the numerical experiment is valid.

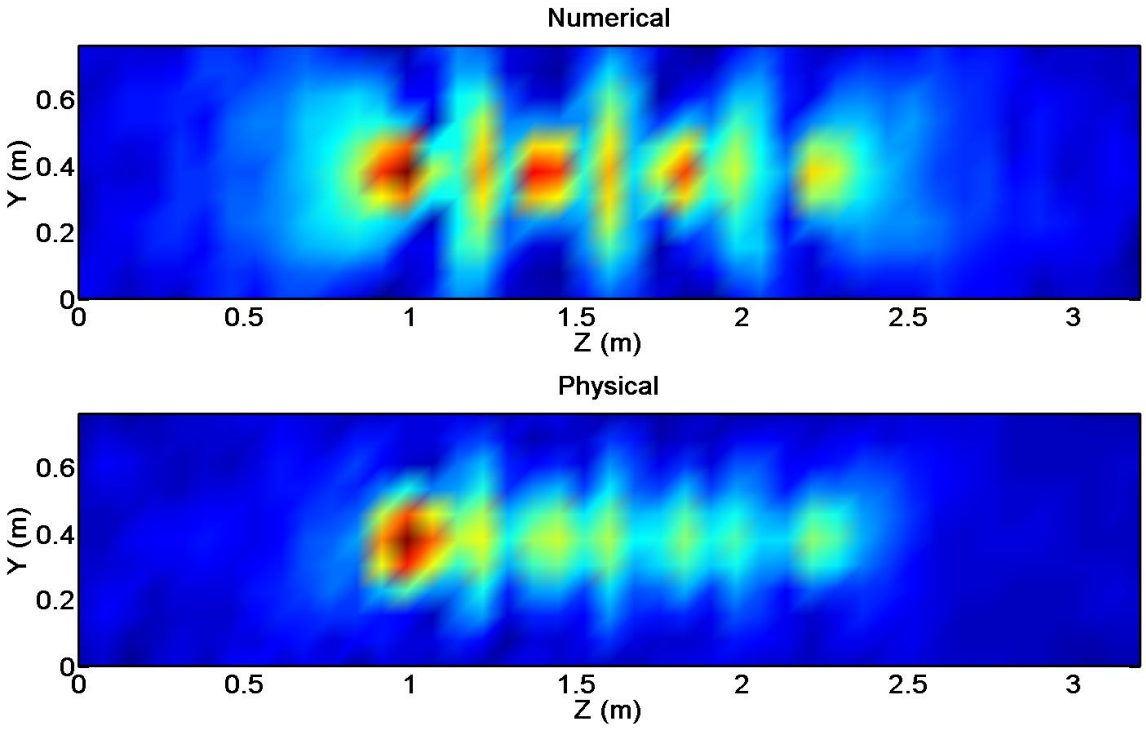

Figure 2-8 Two color plots comparing reconstruction shape results of the physical experiment and the similar numerical experiment (red means higher SPL).

Returning to the numerical experiment, four reference microphones were placed at a multitude of different positions with respect to the sources. Results were poor when the reference microphones were all close to one another. This is expected because in the

limit as the combined distance between microphones goes to zero, the one-reference microphone case is approached which cannot distinguish more than one independent source. The results of this numerical experiment suggest there needs to be a balance: references need to be close enough to sense the sources without being too close to each other. In typical NAH experiments, this requirement is easily satisfied with some common sense from the experimenter. However, it is surprising that the four reference microphones farthest away from the sources still gave accurate results in the physical experiment.

The natural extension of studying discrete partially correlated sources is to examine continuous sources. An intermediate step between the four point sources and the continuous sources is a 20 point source experiment. With 20 partially correlated point sources (the coefficient *b* was 0.7), the relaxed requirement on reference microphone number is even more exaggerated. This was done numerically, with the coherence between all 20 sources shown in Fig. 2-9. Notice that the diagonal is uniformly one because the coherence between a source and itself is one. In addition, notice that the farther downstream (higher source number) the coherence drops off more slowly, as is the case with jet noise.[3]

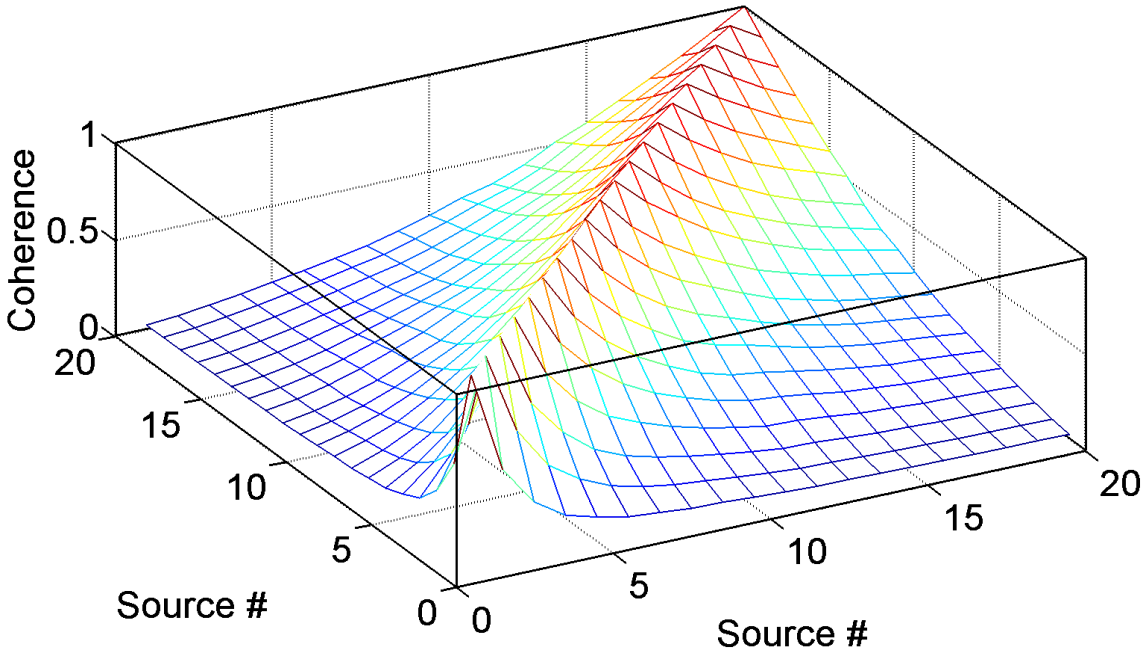

Figure 2-9 Coherence between every pair of sources for the 20 source case (moderately correlated at 900 Hz).

Again, reconstruction errors were investigated as a function of reference microphone number and are displayed in Fig. 2-10 for two different frequencies. It is possible to accurately reconstruct 20 point sources with only nine or ten reference microphones for both cases. Again, the errors do not dramatically decrease by adding reference microphones.

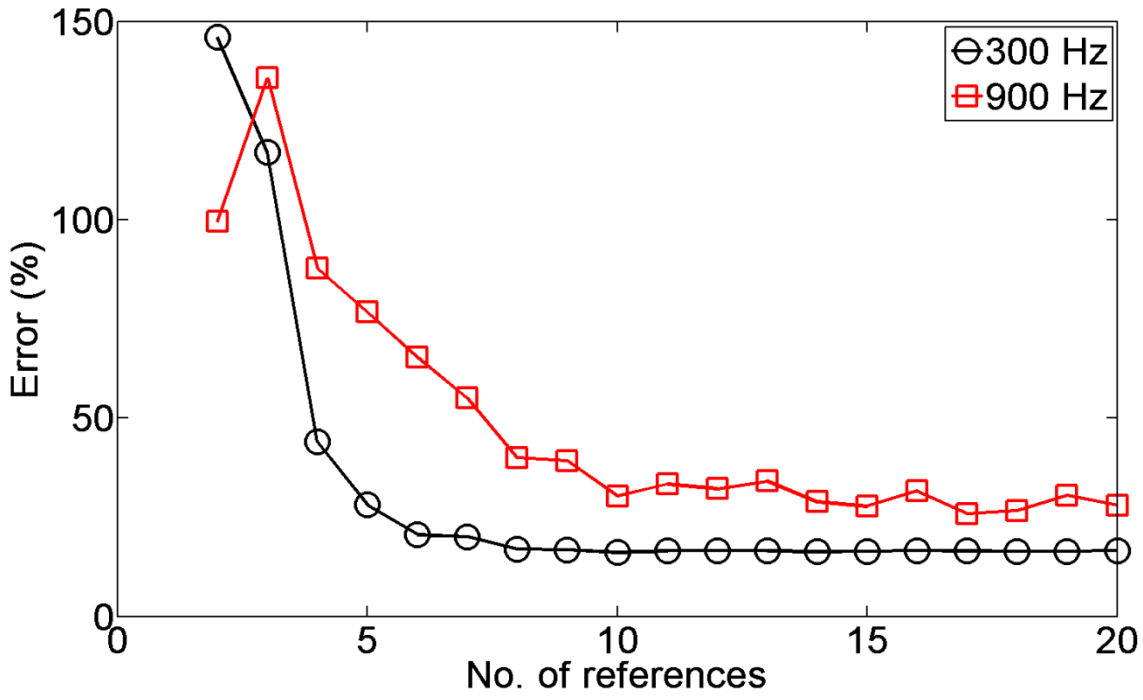

Figure 2-10 Mean percent error as a function of number of reference microphones for 20 numerically generated, moderately correlated point sources and two different frequencies: 300 Hz and 900 Hz.

2.5 Conclusions

In applying scan-based NAH to partially correlated fields, the virtual coherence method has been shown to be effective. With regards to guidelines, reference microphone number and placement are found to be important aspects of the virtual coherence method. However, for a sufficient number of reference microphones, placement is not too critical so long as all the sources are sensed. In addition, four partially correlated sources can be accurately reconstructed with three or fewer reference microphones owing to the linear dependence between the sources, as long as the degree of correlation is high enough. Also, once the critical number of reference microphones is achieved, adding reference microphones will not appreciably decrease the error.

These results may be useful to anyone trying to apply scan-based NAH in cases where the sources are not completely coherent. The original guideline that there must be as many reference microphones as there are independent sources is somewhat misleading. In these experiments, it was shown that four sources, each with a varying combination of four independent signals could be accurately reconstructed with three or even two reference microphones. Granted, the fourth signal was greatly reduced in amplitude, but it was still present (see Eq. 2.17).

There is further research still to be done. In the physical experiment, the reference microphones were ideally located, i.e. they could sense all the sources; another experiment could be performed where the microphones were not ideally located (in addition to a numerical experiment), and more specific guidelines regarding reference location could be given.

References

[1] K. Viswanathan, "Investigation of the sources of jet noise," 13th AIAA/CEAS Aeroacoustics Conference, AIAA Pap. 2007-3601(2007).

[2] D. J. Bodony, "The prediction and understanding of jet noise," Center for Turbulence Research Annual Research Briefs, 367-377 (2005).

[3] R. H. Self, "Jet noise prediction using the Lighthill acoustic analogy," J. Sound Vib. **275**, 757-768 (2004).

[4] C. K. W. Tam, N.N. Pastouchenko, R.H. Schlinker, "Noise source distribution in supersonic jets," J. Sound Vib. **291**, 192-201 (2006).

[5] D. Papamoschou and A. Dadvar, "Localization of multiple types of jet noise sources," 12th AIAA/CEAS Aeroacoustics Conference, Cambrider, MA, AIAA Pap. 2006-2644 (2006).

[6]C. K. W. Tam, K. Viswanathan, K. K. Ahuja, J. Panda, "The sources of jet noise: experimental evidence," 13th AIAA/CEAS Aeroacoustics Conference, AIAA Pap. 2007-3641 (2007).

[7] J. Laufer, R. Schlinker, and R. E. Kaplan, "Experiments on supersonic jet noise," AIAA J. **14** (4) 489-497 (1976).

[8] R. H. Schlinker, S. A. Liljenberg, D. R. Polak, K. A. Post, C. T. Chipman, A. M. Stern, "Supersonic jet noise source characteristics & propagation: engine and model scale," 13th AIAA/CEAS Aeroacoustics Conference, AIAA Pap. 2007-3623 (2007).

[9] H. V. Fuchs, "On the application of acoustic 'mirror', 'telescope', and 'polar correlation' techniques to jet noise source location," J. Sound Vib. **58** (1) 117-126 (1978).

[10] M. Lee, J. S. Bolton, and L. Mongeau, "Application of cylindrical near-field acoustical holography to the visualization of aeroacoustic sources," J. Acoust. Soc. Am. **114** (2) 842-858 (2003).

[11] M. Lee, J. S. Bolton, "Source characterization of a subsonic jet by using near-field acoustical holography," J. Acoust. Soc. Am. **121** (2) 967-977 (2007).

[12] A. Michalke, "Some remarks on source coherence affecting jet noise," J. Sound Vib. **87** (1) 1-17 (1983).

[13] J. D. Maynard, E. G. Williams, and Y. Lee, "Nearfield acoustic holography: I. Theory of generalized holography and the development of NAH," J. Acoust. Soc. Am. **78** (4) 1395-1413 (1985).

[14] R. Steiner and J. Hald, "Near-field acoustical holography without the errors and limitations caused by the use of spatial DFT," Int. J. Sound Vib. **6** (2) 83-89 (2001).

[15] J. Hald, "Patch near-field acoustical holography using a new statistically optimal method," Proc. INTER-NOISE 2003, 2203–2210 (2003).

[16] Y. T. Cho, J. S. Bolton, and J. Hald, "Source visualization by using statistically optimized near-field acoustical holography in cylindrical coordiantes," J. Acoust. Soc. Am. **118** (4), 2355-2364 (2005).

[17] J. Hald, "Basic theory and properties of statistically optimized near-field acoustical holography," J. Acoust. Soc. Am. **125** (4), 2105-2120 (2009).

[18] E. G. Williams, "Regularization methods for near-field acoustical holography," J. Acoust. Soc. Am. **110** (4), 1976-1988 (2001).

[19] E. G. Williams, "Approaches to patch NAH," Proc. INTER-NOISE **03** 2187-2194 (2003).

[20] J. Hald, "STSF – A unique technique for scan-based near-field acoustic holography without restrictions on coherence," B&K Technical Review No. 1 (1989).

[21] I. T. Joliffe, *Principal Component Analysis*, (Springer-Verlag New York, Inc., 2002).

[22] D. L. Hallman and J. S. Bolton, "A comparison of multi-reference nearfield acoustical holography procedures," Proc. NOISE-CON **94** 929-934 (1994).

[23] H. -S. Kwon and J. S. Bolton, "Partial field decomposition in nearfield acoustical holography by the use of singular value decomposition and partial coherence procedures," Proc. NOISE-CON **98** 649-654 (1998).

[24] K. -U. Nam and Y. -H. Kim, "Visualization of multiple incoherent sources by the backward prediction of near-field acoustical holography," J. Acoust. Soc. Am. **109** (5) 1808-1816 (2001).

[25] K. -U. Nam and Y. -H. Kim, "A partial field decomposition algorithm and its examples for near-field acoustical holography," J. Acoust. Soc. Am. **116** (1) 172-185 (2004).

[26] H. -S. Kwon, Y. -J. Kim, and J. S. Bolton, "Compensation for source nonstationarity in multireference, scan-based near-field acoustical holography," J. Acoust. Soc. Am. **113** (1) 360-368 (2003).

[27] M. Lee and J. S. Bolton, "Scan-based near-field acoustical holography and partial field decomposition in the presence of noise and source level variation," J. Acoust. Soc. Am. **119** (1) 382-393 (2006).

[28] H. Van der Auweraer and L. Hermans, "Multivariate correlation analysis of nonstationary signals: application to pass-by-noise problems," ICASSP '00 3903-3906 (2000).

[29] D. Long, J. Peters, and M. Anderson, "Evaluating turbofan exhaust noise and source characteristics from near field measurements," 15th AIAA/CEAS Aeroacoustics Conference, Miami, FL, AIAA Pap. 209-3214 (2009).

[30] D. Otte, P. Sas, P. Van de Ponseele, "Noise source identification by use of principal component analysis," Proc. INTER-NOISE 88, 199-202 (1988).

[31] J. S. Bendat and A. G. Piersol, *Random Data: Analysis and Measurement Procedures*, (John Wily & Sons, Inc., New York, 2000).

CHAPTER 3

SCAN-BASED NEAR-FIELD ACOUSTICAL HOLOGRAPHY ON CONTINUOUS, PARTIALLY CORRELATED SOURCES

3.1 Introduction

The characterization of the noise sources in jet engine exhaust has been a challenge since the 1950s.[1] Because of the difficulties of directly measuring the turbulence within supersonic, heated jet flows, the use of acoustical inverse methods to deduce equivalent source properties has been explored. Although far-field phased array methods[2-6] have been most often used in jet noise source characterization, there have been recent efforts to apply near-field acoustical holography (NAH) to jet noise[7-8] and other aeroacoustic sources.[9]

There are challenges to the application of NAH to a jet. The combination of distributed spatial extent and the desire to resolve the source location for both low and high frequencies can result in a prohibitive number of microphones. Scan-based NAH [e.g., see Ref. 10] could alleviate the need for such a large number of microphones, but has traditionally required a coherent source so that the relative phases between measurement locations can be measured using a stationary reference microphone. Aeroacoustic sources are not fully coherent and therefore present a problem to scan-based NAH.

Partial field decomposition allows one to perform scan-based NAH on fields without restrictions on coherence.[10] The key to this technique is the use of multiple stationary reference microphones. Guidelines for reference microphone number and

placement have been to have as many references as there are independent sources and such that the references sense all the sources. These criteria are not necessarily sufficient because they are not straightforward to determine for jet noise because of the continuously distributed and partially correlated nature of the source region.

Many have investigated the coherence of jet noise.[11-16] An important discovery they have made is that source coherence/interference (axial interference specifically) is a primary determinant of jet noise directivity.[12] Coherence length of a jet is also found to be a function of frequency and axial position in the jet.[15] Higher frequencies and positions farther upstream correspond to shorter coherence lengths. This is because fine scale turbulence, occurring more upstream, is associated with higher frequencies and shorter coherence lengths due to the smaller scale of the turbulence; conversely, large scale turbulence, occurring more downstream, is associate with low frequency radiation and greater coherence lengths for the opposite reason.[17] Furthermore, the radial and azimuthal components of jet noise coherence have also been studied, and it has been shown that these components do contribute significantly to the far field radiation characteristics.[11-12] This chapter will restrict attention to axial coherence effects in the numerical experiment.

In Chapter 2, results from physical and numerical experiments on controlled discrete partially correlated sources were presented. Results from those experiments demonstrated that fewer reference microphones than physical sources were required if the sources were partially correlated. Also, having the required number of reference microphones was found to be more important than their placement in determining

reconstruction error. One question still unanswered is: what are the guidelines for reference microphones in a partially correlated, continuously distributed source?

This chapter will investigate reference microphone number and coherence length and the resultant NAH reconstruction error and mean virtual coherence sum. The numerical experiments are designed to mimic certain accepted jet noise source characteristics. Specifically, the spatial variation of source amplitude and the continuous and partially correlated nature of jet noise will be incorporated into the numerical experiment. In addition, total source length will be investigated in terms of number of coherence lengths. Furthermore, reference microphone window-like effects will be briefly investigated (window-like and not window effects because window effects are traditionally associated with the Fourier transform). A final note on coherence as it relates to propagation delay will be given as well. All these aspects will be examined to see how they contribute to reconstruction error which permits us to give better guidelines for reference microphone number and placement in preparation for performing scan-based NAH with a limited number of reference microphones. This exercise is particularly useful given the spatial extent of the noise source region in, e.g., the jet produced by a high-performance military aircraft.

3.2 Experiment

3.2.1 Background

Rather than giving a detailed description of scan-based NAH and the virtual coherence method, the reader is referred to Chapter 2 for more details. However, the overall process is worth summarizing. A measurement is made on a hologram surface that is

ideally in the near field of the source. For this problem, scan-based NAH is required (owing to the size of full-scale jets) necessitating partial field decomposition (because of the lack of coherence) in conjunction with virtual coherence. The virtual coherence method separates an incoherent field into coherent partial fields which are mutually incoherent. These partial fields are then processed using NAH (SONAH in this case[18]) and then reconstructed on a surface closer to the source or elsewhere, if desired. These partial fields can then be added on an intensity basis to get total magnitude on the reconstruction surface.

In any attempt to do a problem of a continuous nature numerically, some degree of discretization is necessary. In the experiment, 100 point sources were generated in a line and spaced closely enough (according to the dimensions of the problem) to be practically considered a continuous source. The sources were spaced 1.2 cm apart each, small compared to the wavelengths at 300 Hz and 900 Hz which were 87.5 cm and 38.1 cm, respectively. It was concluded that they were spaced closely spaced enough when adding more sources did not noticeably affect the results. The setup or geometry of the experiment is shown in Fig. 3-1.

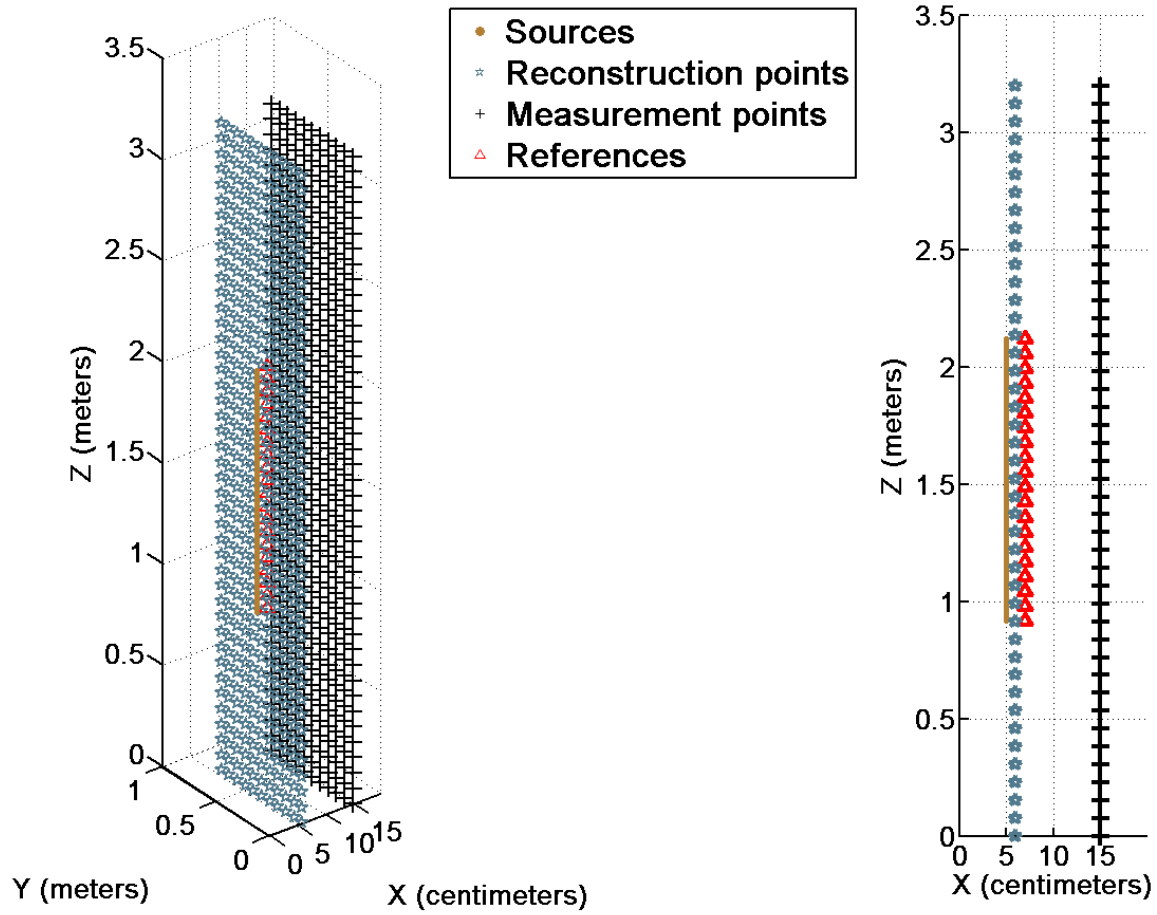

Figure 3-1 Diagrams from two different views showing the relevant numerical experiment geometry (not to scale) with sources, reconstruction and measurement points, and references (only 20 are shown here).

The sources were generated in the frequency domain (time independent) using the free-space Green's function with complex amplitude. The pressure at some field point $\vec{r}$ was calculated via Eqs. 3.1 and 3.2.

$$\hat{p}(\vec{r}) = \sum_{i=1}^{N} \hat{A}_i \, G\left(\vec{r}|\vec{r}_{0_i}\right), \tag{3.1}$$

and

$$G(\vec{r}|\vec{r}_0) = \frac{e^{-jk\,|\vec{r}-\vec{r}_0|}}{|\vec{r}-\vec{r}_0|}. \tag{3.2}$$

Here $\widehat{A}$ is the complex amplitude, N is the number of sources, G is the free-space Green's function and $\vec{r}$ and $\vec{r}_0$ represent the vectors pointing to the field point and source point respectively. This complex amplitude was varied in an appropriate manner (given by Eq. 3.3) across the sources, scans, and blocks in order to obtain different degrees of correlations: moderately correlated and highly correlated. The source amplitude $\widehat{A}_{\text{source }1}$ is just $\widehat{A}_{\text{signal }1}$; the other source amplitudes are given as

$$\hat{A}_{source\ i} = \hat{A}_{source\ i-1} + b \times \hat{A}_{signal\ i} \; for\; i = 1, 2, \ldots, Q. \tag{3.3}$$

In Eq. 3.3, Q represents the total number of sources, 100 in this case. $\hat{A}_{source\ i}$ and $\hat{A}_{source\ i}$ are actually matrices of complex amplitudes across all the scans and blocks for that source. This is necessary because a single block cannot predict a coherence less than one.[10] In fact, the magnitudes of the complex amplitudes had a normal distribution truncated at zero and the phase was uniformly distributed between -π and π. This was also how the discrete numerical sources of Chapter 2 were generated. There were always ten more blocks then there were references. This ensured that the number of references (not the number of blocks) was the limiting factor for detecting the independent sources.

Reference microphones were simulated in a line two centimeters away from the sources. The spacing of the microphones depended and how many there were (anywhere from 2 to 50). The first one was always at 0.92 meters in the z-direction and the last one was always at 2.12 meters according to the grid shown in Fig. 3-1. The measurement grid was simulated 10 cm away from the sources and consisted of an 11 x 43 grid broken up into 43 scans of an 11 microphone array. Reconstructions were made on a similar grid one centimeter away from the sources (see Fig. 3-1). A set of color plots showing the measured, reconstructed, and benchmark SPLs in addition to the sum of partial fields is shown in Fig. 3-2. The measured plot in Fig. 3-2a looks smoother compared to that of the previous chapter (Fig. 2-4a). This is due to the increase in the number of averages (60 as opposed to 18). The number of references used was 50. The sum of the partial fields (Fig. 3-2b) still smoothes out some of the discontinuities still present in the measured plot. Reconstructed (Fig. 3-2c) and benchmark (Fig. 3-2d) plots are shown as well.

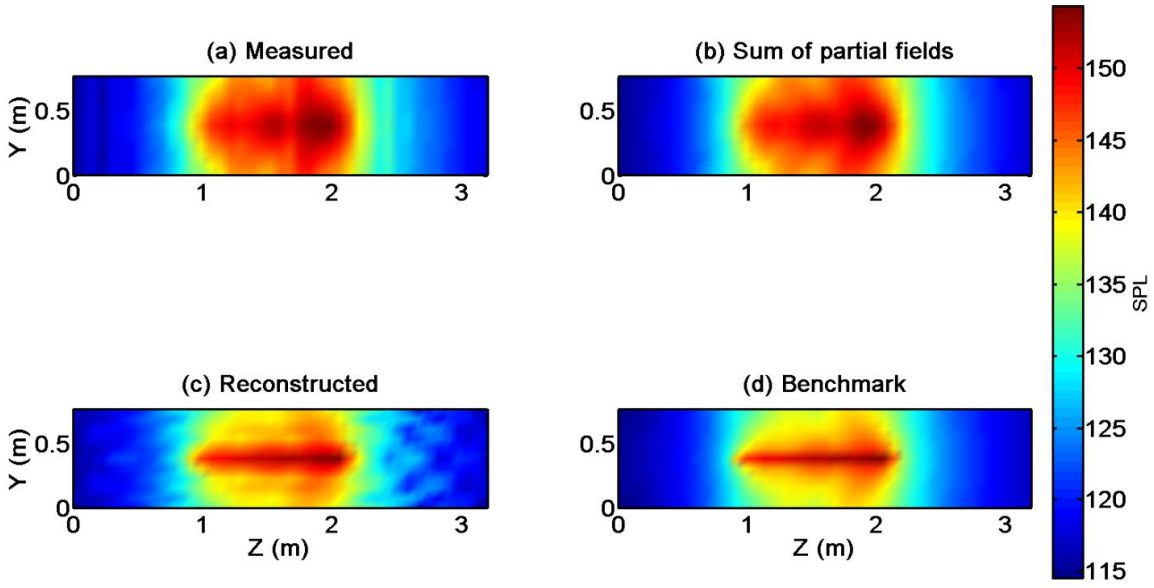

Figure 3-2 Color plots in SPL of (a) measured- averaged over all blocks at 37.5 cm (b) the sum of partial fields- measured at 37.5 cm (c) SONAH reconstructed at 7.5 cm (d) benchmark-measured at 7.5 cm . All plots are for 900 Hz.

The percent error between the numerically generated benchmark result and the reconstruction was calculated as

$$mean\ error\ (\%) = \sqrt{\frac{\sum_i |p_{t,i} - p_{s,i}|^2}{\sum_j |p_{t,j}|^2}} (\times 100), \tag{3.4}$$

where p_t is the actual pressure and p_s is the reconstructed pressure.[18]

3.2.2 Reference microphones per coherence length

In order to achieve consistency across varying degrees of correlation, a new figure of merit was created: reference microphones per coherence length (rpl_c). This figure of merit was chosen because it is generalized across different degrees of correlation and

frequency. It will help guide reference microphone placement and quantity for a more complicated situation. Determining the number of reference microphones per coherence length requires the calculation of coherence between reference microphones, which is via the following Eq. 3.5.

$$\gamma^2 = \frac{|C_{ij}|^2}{C_{ii}C_{jj}}. \tag{3.5}$$

In Eq. 3.5, C_{ij} represents the cross spectrum between the *i*th and *j*th reference microphones and C_{ii} and C_{jj} represent their respective autospectra. For this experiment, the coherence length was defined as the distance (moving in the positive z-direction in Fig. 3-1) where the coherence between reference microphones dropped to 0.5. This definition of coherence length is arbitrary, but while other definitions of coherence length are possible (and also arbitrary), the present one is simple both to implement and to understand. A linear interpolation was used between microphones to approximately determine where the coherence dropped to 0.5. This figure of merit is also a function of distance because the coherence length increases as one moves in the positive z-direction across the sources. This mimics the coherence characteristics of jets as the larger coherent eddy structures are more prevalent downstream.[15]

The simulation was run with 13 different numbers of reference microphones (from 2 to 50), two different degrees of correlation (moderate and high), and two different frequencies (300 and 900 Hz). For the moderately correlated case, in Eq. 3.3, *b* was equal to 0.7 while *b* was 0.23 for the highly correlated case. The percent error versus rpl_c is shown in Fig. 3-3 in addition to the mean virtual coherence sum.

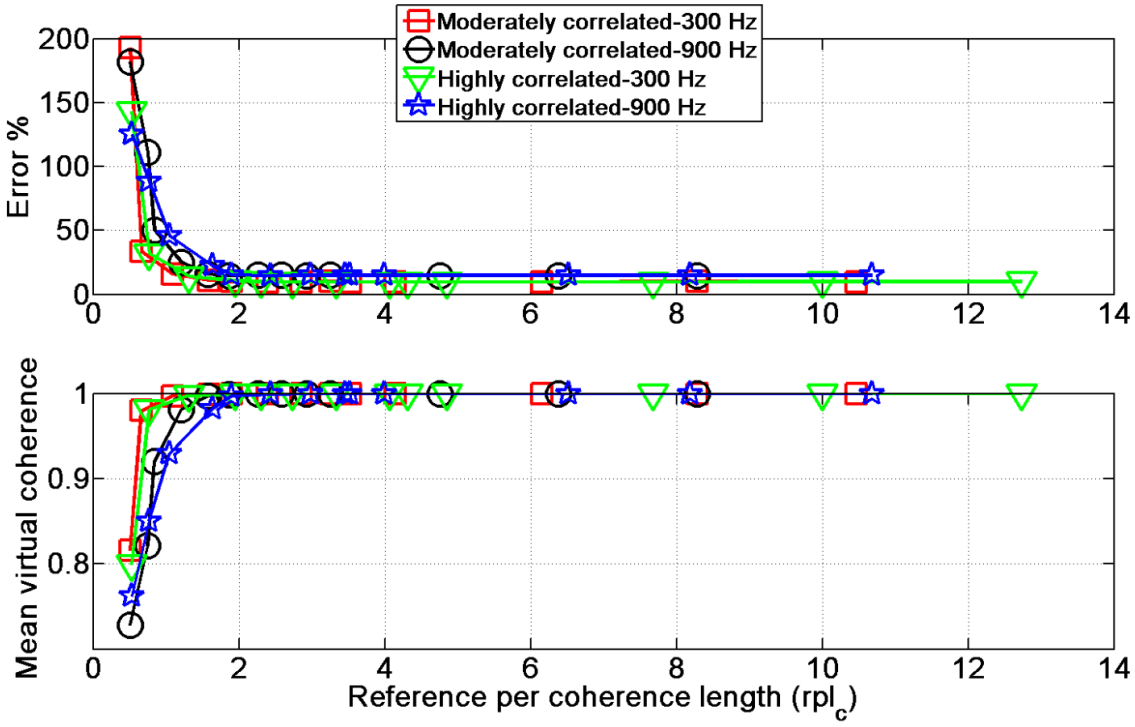

Figure 3-3 Graph depiction of percent error (top) and mean virtual coherence sum (bottom) as a function of the new figure of merit, reference microphones per coherence length (rpl_c), for two different frequencies and two different correlation strengths.

The coherence length in this figure of merit represents the *average* coherence length for all the reference microphones. The average is emphasized only because the coherence length varied as a function of position, and not because of any irregular reference microphone spacing. Figure 3-4 shows the variation in coherence length as a function of position. Note the reference microphones are linearly spaced and it is the coherence length that changes with position.

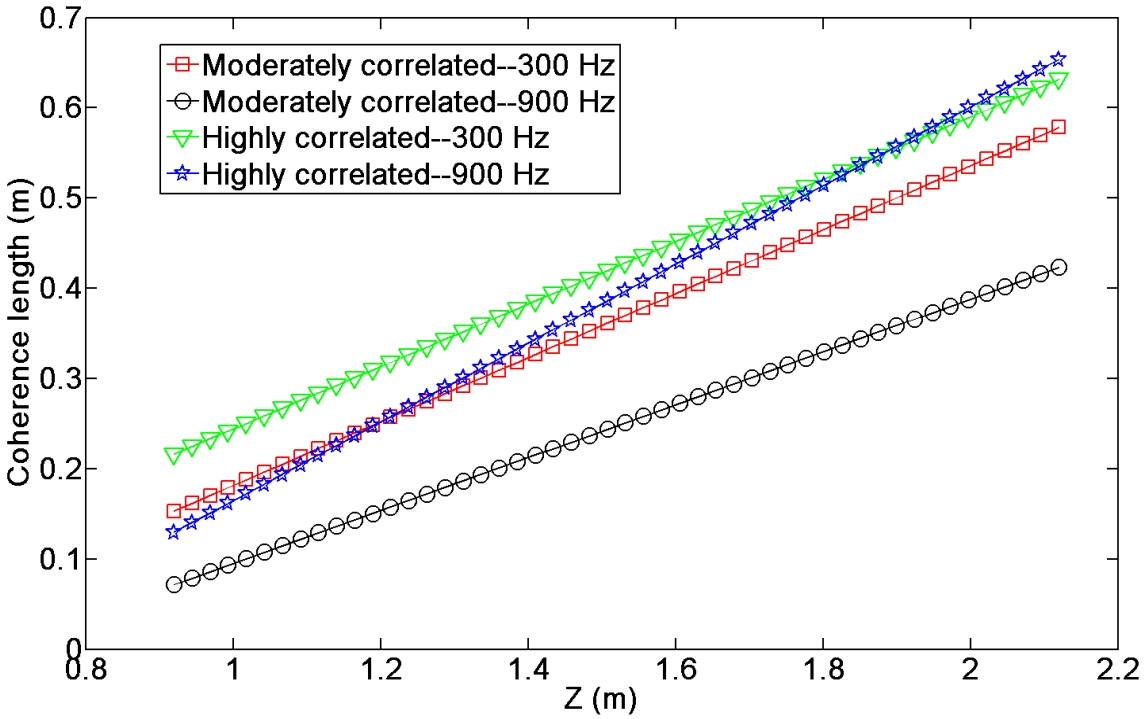

Figure 3-4 Coherence length as measured by the reference microphones in the case with 50 reference microphones for two different degrees of correlation and two different frequencies.

Returning to Fig. 3-3, the percent error approaches its minimum value asymptotically (each frequency has its own minimum error) at approximately 2 rpl_c. The same trend occurs for the mean sum of the virtual coherence, except that it approaches the value of 1 as the rpl_c approaches the value of 2. As the mean sum of the virtual coherence asymptotically approaches 1, error asymptotically approaches a minimum. Going below 2 rpl_c, the error between actual and reconstructed fields grows drastically. Conversely, increasing the number of references beyond 2 rpl_c does not decrease the error. Note that this criterion of two references per coherence length is a rough guideline and specific to this particular definition of coherence length. If different coherence

lengths were chosen, a higher or lower rpl_c was found, but the relationship was not linear. For example, if the coherence length was defined as the distance it takes for the coherence to drop to 0.25, the minimum rpl_c was not found to be 4 (twice the original rpl_c). Furthermore, the coherence was evaluated across the reference microphones (as opposed to the sources) because in a real jet, the coherence will not be known *a priori* and it is the reference microphones that are critical to the virtual coherence and NAH implementation. Therefore, in these tests with reference microphones in a line array, if there are two per coherence length, the reference microphone quantity can be considered sufficient.

Certain assumptions have been made in connection with this result. It is assumed that all the requirements of the NAH are met. This means that the setup must have appropriate grid size, spacing, off-set distance, etc., according to the guidelines for NAH.[20] In other words, if the NAH setup is poor from the start, it does not matter how many reference microphones are used or where they are placed, the results will be poor regardless. The reference microphones should be at an appropriate distance from the sources to sense them all. As a comparison, several different source line to reference line distances were used that were reasonable (2 cm to 20 cm), and the results still dictated 2 rpl_c as the guideline. In addition, the experiment was repeated with 300 point sources and was more than double the length of the 100 point source array. The length of the reference microphone array and measurement grid was scaled accordingly as well. Again, the results were the same, independent of how many coherence lengths the source was in length, which suggests that these results are general for partially correlated noise sources for this definition of coherence length.

3.2.3 Spatial variation in amplitude

Another aspect of jet noise is the dependence of source amplitude upon frequency and position.[13,21] Higher frequencies originate closer to the nozzle and lower frequencies, farther from the nozzle.[17] A simple investigation as to how spatial variation of amplitude affects reference microphone placement was deemed appropriate. Is it advantageous to place more reference microphones in high-amplitude regions? Previous experiments (those in Chapter 2) with discrete physical sources suggest it is not advantageous (did not matter where reference microphones were placed), but these did not exhibit the high spatial variation in amplitude that noise sources in heated, supersonic jets exhibit.[17]

In order to perform the investigation of a spatially varying source amplitude, the source amplitude was varied according to a Gaussian curve (not exactly what occurs in jets, but is simple to implement and a reasonable approximation) as

$$q = ae^{-\frac{(x-b)^2}{2c^2}}, \tag{3.6}$$

where q is the source amplitude, x is the position along the axis, and a, b, and c are constants. The constant b is the center or peak of the Gaussian. The experiment was repeated for two different situations: where the peak was 3/4 of the way downstream and where the peak was 1/4 of the way downstream. Fig. 3-5 is a stem plot showing the reference microphone SPL averaged over blocks and scans for four different cases. Each stem represents a different reference microphone. Here the source region was extended to 3.2 meters in length. Figures 3-5a and 3-5c show linear spacing of reference microphones for both source amplitude functions (3/4 downstream and 1/4 downstream). Figures 3-4b and 3-4d show the same source amplitude functions with denser reference

microphone spacing where the source amplitudes are higher and sparser spacing in the low amplitude region (same number of microphones total). In all four cases of Fig. 3-4, the 2 rpl_c requirement was met. The result is that the errors are decreased when additional microphones are placed in regions of higher amplitude. Therefore, for this test case, it is advantageous to put more reference microphones in higher amplitude areas when the source amplitude varies spatially as measured by the reference microphones. With the peak source acoustic power location being a function of frequency, it makes sense to place more reference microphones in regions of high acoustic power for the specific frequencies of interest. This comes back to the original guideline that the microphones need to sense all the sources; placing microphones in the wrong locations is inefficient.

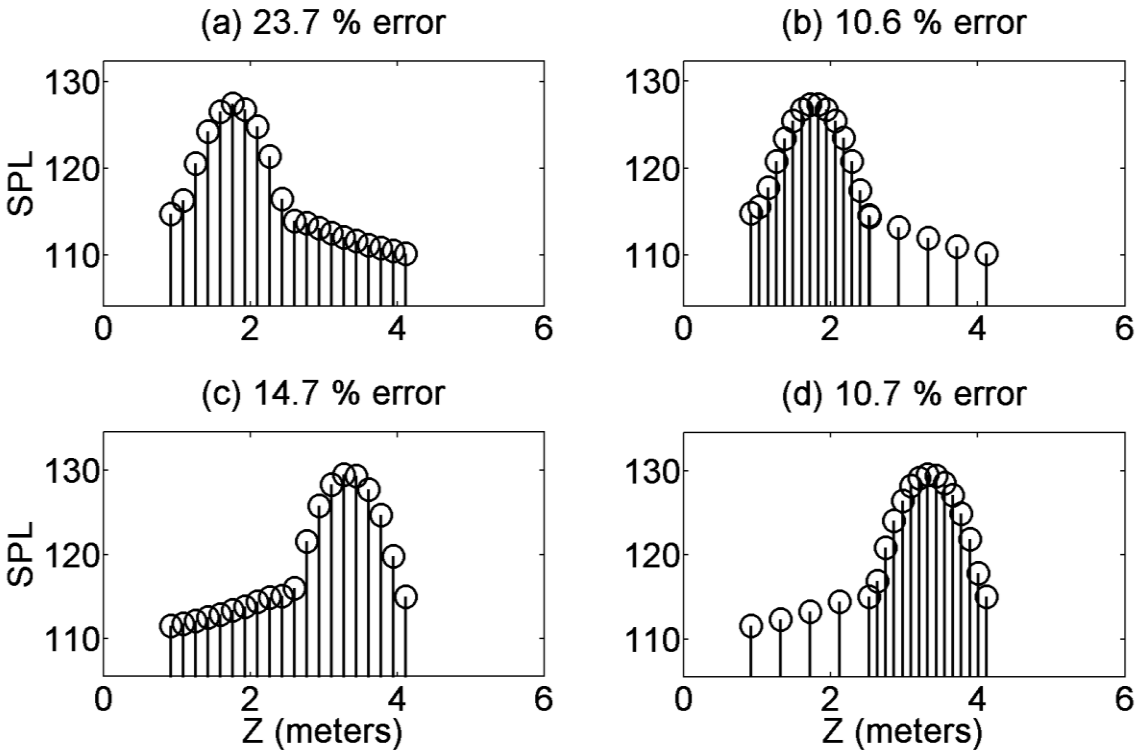

Figure 3-5 Stem plots representing reference microphones averaged over blocks and scans. (a) Uniform spacing with higher source amplitude on the left (1/4 downstream) showing 23.7% error. (b) Denser spacing at the higher source amplitude on the left (1/4 downstream) showing 10.6% error (c) Uniform spacing with higher source amplitude on the right (3/4 downstream) showing 14.7% error (d) Denser spacing at the higher source amplitude on the right (3/4 downstream) showing 10.7 % error.

3.3 Discussion

With the test cases given in the previous section, it is useful to have a discussion of their results as they pertain to practical reference microphone guidelines. There should be enough reference microphones to have two per average coherence length. Keep in mind these results are for a coherence length defined as the distance at which the coherence

between two microphones has dropped to 0.5. Other definitions of coherence length may yield a different criterion, but they should still be general across frequency, degree of correlation, and overall length of source.

If the source power varies spatially and there are enough reference microphones per coherence length, extra microphones should be placed in regions of high power in order to further decrease errors (or reference microphones could be swapped from low-amplitude regions to high-amplitude regions). Note that after reaching 2 rpl_c, additional microphones did not reduce the error. However, that was for a uniform source amplitude distribution; additional microphones can still reduce error when significant spatial variation exists. With higher frequencies originating more upstream and lower frequencies originating more downstream, and the different directivities associated with these frequencies, a broadband application of NAH is difficult because it is problematic to try and position the reference microphones ideally for all frequencies. A compromise is necessary, unless one can narrow the frequency range of interest to a more defined region. These guidelines presume that the NAH grid is positioned properly with respect to the source with enough measurement points and a large enough grid size to avoid window-like effects (although SONAH alleviates the latter requirement to some extent[20]).

3.3.1 Range in reference microphone SPL

Another experiment was designed to help an experimenter answer the question: are the reference microphones adequately capturing the entire, extended length of the source region? It has been found that a drop-off of 6 dB or more between the peak amplitude and the edge reference microphone amplitude is sufficient to avoid window-like effects in the reference microphones. The same 100 point sources were used with 20 reference

microphones. The reference microphone array was centered at the center of the source array but was varied in length from one half to one times the length of the source array. The shorter reference array limited the amount that the averaged SPL could drop from the peak to the ends of the reference array (not adequately capturing the entire source region). Note that this experiment assumes a smoothly varying source (no nulls). The error (%) was calculated as a function of the range of average SPL in dB across all the reference microphones. As seen in Fig. 3-6, once a range of about 6 dB is reached between maximum and minimum SPL, the error is minimized.

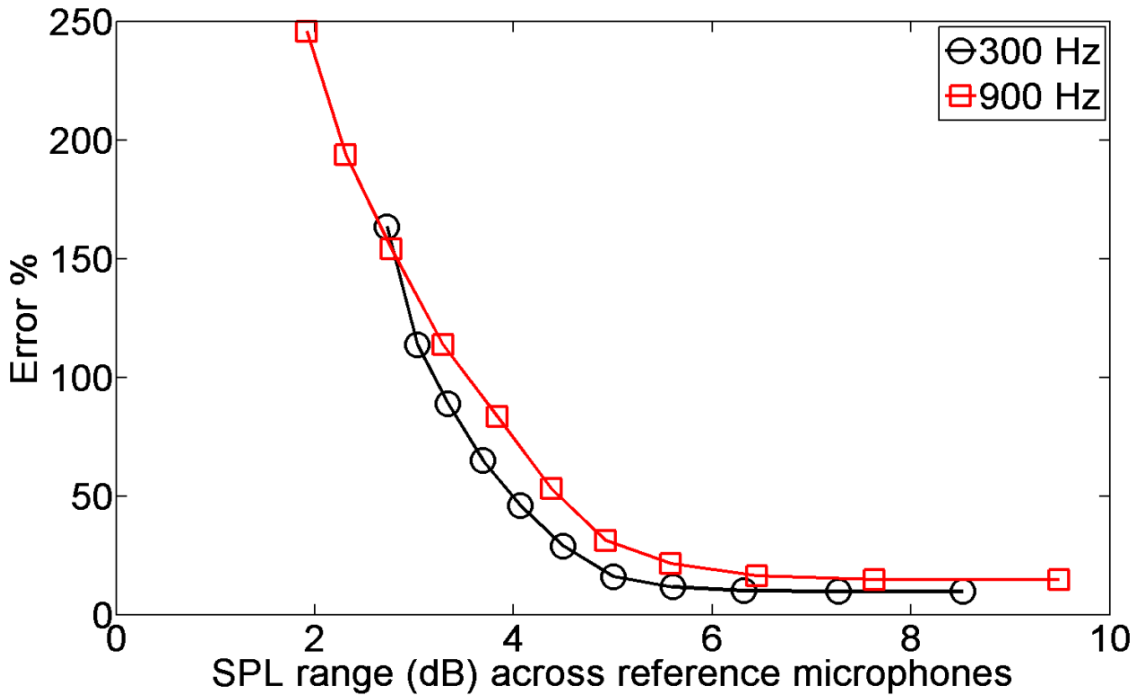

Figure 3-6 Error as a function of range in dB (difference between maximum and minimum SPL) across the reference microphones for two frequencies: 300 Hz and 900 Hz.

3.3.2 Coherence and block size

In tests on a full-scale military aircraft jet, the distances between the farthest pair of microphones can be on the order of 30 meters or more. To ensure proper coherence between these microphones, care must be taken to make certain that the propagation delay between reference microphones and measurement microphones is accounted for in the cross-spectral matrices.[22] If the propagation delay is not accounted for, poor coherence will usually be the result. For example, an acoustic signal at a reference microphone will be coherent with an acoustic signal at a field microphone after a finite amount of time as the sound travels the distance between the two microphones. (This issue was not a concern in these numerical experiments since the signals were all generated in the frequency domain (time-independent) via Eqs. 3.1 and 3.2).

This effect can be accounted for in two ways: have a large enough block size to account for the delay, or implement a constant average delay. Implementing individual reference microphone to measurement microphone delays is infeasible since NAH requires a coherent map and the specific delays will appear as a different source to NAH. The latter also effectively moves the reference microphones from scan to scan, which violates the requirement that they be stationary. Having a large enough block size seems to be the easiest approach to deal with this issue.

3.4 Conclusions

In numerical experiments with distributed partially correlated sources, it has been shown that the reference microphone per coherence length figure of merit is useful to gauge reconstruction errors. With a coherence length defined as the distance it takes for the

coherence to drop to 0.5, a guideline of at least two reference microphones per coherence length was found to minimize reconstruction errors. This guideline was found to be independent of frequency, correlation strength, source length, and reasonable reference to source distances. For a source with a spatially varying amplitude, having additional microphones in the high amplitude region was also found to reduce reconstruction errors. A reference microphone drop-off of 6 dB was found to be sufficient to fully capture the source and avoid reconstruction errors. It is also important to have good coherence between reference and measurement microphones, which requires proper accounting of the propagation delay between them.

References

[1] M. J. Lighthill, "On sound generated aerodynamically. I. General theory," Proc. R. Soc. Lond. A **211**, 564-587 (1952)

[2] H. V. Fuchs, "On the application of acoustic 'mirror', 'telescope', and 'polar correlation' techniques to jet noise source location," J. Sound Vib. **58** (1) 117-126 (1978).

[3] D. Papamoschou and A. Dadvar, "Localization of multiple types of jet noise sources," 12th AIAA/CEAS Aeroacoustics Conference, Cambrider, MA, AIAA Pap. 2006-2644 (2006).

[4] D. Papamoschou, P. J. Morris, and D. K. McLaughlin, "Beamformed flow-acoustic correlations in high-speed jets," 15th AIAA/CEAS Aeroacoustics Conference, Miami, FL, AIAA Pap. 2009-3212 (2009).

[5] J. Billingsley and R. Kinns, "The acoustic telescope," J. Sound Vib., **48** (4) 485-510 (1976).

[6] M. J. Fisher, M. Harper-Bourner, and S. A. L. Glegg, "Jet engine source location: the polar correlation technique," J. Sound Vib. **51** (1) 23-54 (1977).

[7] M. Lee, J. S. Bolton, "Source characterization of a subsonic jet by using near-field acoustical holography," J. Acoust. Soc. Am. 121 (2) 967-977 (2007).

[8] D. Long, J. Peters, and M. Anderson, "Evaluating turbofan exhaust noise and source characteristics from near field measurements," 15th AIAA/CEAS Aeroacoustics Conference, Miami, FL, AIAA Pap. 209-3214 (2009).

[9] M. Lee, J. S. Bolton, and L. Mongeau, "Application of cylindrical near-field acoustical holography to the visualization of aeroacoustic sources," J. Acoust. Soc. Am. **114** (2) 842-858 (2003).

[10] J. Hald, "STSF – A unique technique for scan-based near-field acoustic holography without restrictions on coherence," B&K Technical Review No. 1 (1989).

[11] A. Michalke, "Some remarks on source coherence affecting jet noise," J. Sound Vib. **87** (1) 1-17 (1983).

[12] U. Michel, "The role of source interference in jet noise," 15th AIAA/CEAS Aeroacoustics Conference, Miami, FL, AIAA Pap. 2009-3377 (2009).

[13] K. Viswanathan, "Investigation of the sources of jet noise," 13th AIAA/CEAS Aeroacoustics Conference, AIAA Pap. 2007-3601 (2007)

[14] L. Masestrello, "Statistical properties of the sound and source fields of an axisymmetric jet," AIAA Pap. 77-1267 (1977)

[15] R. H. Self, "Jet noise prediction using the Lighthill acoustic analogy," J. Sound Vib. **275**, 757-768 (2004).

[16] R. R. Armstrong, H. V. Fuchs, and A. Michalke, "Coherent structures in jet turbulence and noise," J. AIAA **15** (7) 1011-1017 (1977).

[17] C. K. W. Tam, K. Viswanathan, K. K. Ahuja, J. Panda, "The sources of jet noise: experimental evidence," 13th AIAA/CEAS Aeroacoustics Conference, AIAA Pap. 2007-3641 (2007).

[18] J. Hald, "Basic theory and properties of statistically optimized near-field acoustical holography," J. Acoust. Soc. Am. **125** (4), 2105-2120 (2009).

[19] Y. T. Cho, J. S. Bolton, and J. Hald, "Source visualization by using statistically optimized near-field acoustical holography in cylindrical coordinates," J. Acoust. Soc. Am. **118** (4), 2355-2364 (2005).

[20] R. Steiner and J. Hald, "Near-field acoustical holography without the errors and limitations caused by the use of spatial DFT," Int. J. Sound Vib. **6** (2) 83-89 (2001).

[21] R. H. Schlinker, S. A. Liljenberg, D. R. Polak, K. A. Post, C. T. Chipman, A. M. Stern, "Supersonic jet noise source characteristics & propagation: engine and model scale," 13th AIAA/CEAS Aeroacoustics Conference, AIAA Pap. 2007-3623 (2007).

[22] J. S. Bendat and A. G. Piersol, *Random Data: Analysis and Measurement Procedures*, (John Wily & Sons, Inc., New York, 2000).

CHAPTER 4

CONCLUSIONS

In applying scan-based NAH to partially correlated fields, the virtual coherence method has proven to be effective. Reference microphone number and placement are found to be important aspects of the virtual coherence method. However, given a certain number of reference microphones, placement is not too critical so long as all the sources are sensed. Nonetheless, at extremes (references packed close together), the errors will increase to unacceptable levels. In addition, four partially correlated sources can be accurately reconstructed with three or fewer reference microphones owing to the linear dependence between the sources. Also, once the critical number of reference microphones is achieved, adding reference microphones will not appreciably decrease the error. Further study into reference microphone guidelines with more detailed jet noise based models is warranted.

In numerical experiments with continuous partially correlated sources, it has been shown that the reference microphone per coherence length figure of merit is useful to gauge reconstruction errors. With a coherence length defined as the distance it takes for the coherence to drop to 0.5, a guideline of approximately two reference microphones per coherence length was found to minimize reconstruction errors. This guideline is independent of frequency, degree of correlation, source length, and for distances between reference microphones and sources. In addition, for a source with a spatially varying amplitude, having more microphones in the high amplitude region was also found to reduce reconstruction errors. In another experiment, a reference microphone SPL range

of 6 dB was found to be sufficient to avoid window-like errors in the reference microphones. Furthermore, it is important to have good coherence between all pairs of microphones, which requires one to account for the propagation delay between them.

Further research will include results of an actual test on a full-scale military aircraft jet. It is anticipated that NAH will be better than other phased array methods such as beamforming especially for the large-scale turbulence noise which is at lower frequencies. A comparison between beamforming and NAH performance on jets would be a valuable study. An investigation comparing SONAH to other NAH methods such as patch Fourier NAH or HELS would be beneficial. It is anticipated that the guidelines provided herein will facilitate the application of scan-based NAH with partial field decomposition to full-scale jet tests and to any other problems involving partially correlated sources.

APPENDIX

VIRTUAL COHERENCE

```
%% Clearing, closing
clear
close all
indref=1;
% for x_ref=linspace(.003,1,10);
%     close all
%% Initializing Variables
ind_end=1;
c=343;                                          % Speed of sound
pc=3;                                           % 0 for fully correlated,1
for partially correlated, 2 for uncorrelated, 3 for highly correlated
lin=1;                                          % Linear reference mic
spacing? 1 for yes,
rrr=50;
fvect=900;
fint=fvect;           % Frequency of interest

close all
clear global U1 G1 V1 A alpha U G V
clear refvect references Crrc
Numsources=100;                                  % Number of stationary
sources
scans=43;                                       % Number of scans

meas_z=1;                                       % Number of measurement
microphones on grid in z direction
meas_y=11;                                      % Number of measurement
microphones on grid in y direction
rcs_z=43;                                       % Number of reconstruction
points in z
rcs_y=11;                                       % Number of reconstruction
points in y

refvect=1:rrr;                                  % Number of reference
microphones
references=length(refvect);
blocks=references+10;                           % Number of  blocks
(averages)
x_ref=.02;                                      % Location of reference
microphones in x (distance from source axis)
x_meas=.1;                                      % Location of measurement
microphones in x
x_rcs=.01;                                      % Location of recons.
points in x

y_meas=linspace(0,.762,meas_y);                 % Location of measurement
microphones in y
```

```
y_rcs=linspace(0,.762,rcs_y);               % Locatino of
reconstruction points in y
zstart=.92;                                 % Position of first source
zend=2.12;                                  % Position of last source

z_scan_start=0;                             % First scan position in z
(first mic)
z_scan_end=3.2004;                          % End scan position in z
(last mic)
zmid=(zend+zstart)/2;                       % Calculation of source
midpoint
zfactor=1;                                  % Size of ref. array
compared to source array
zrefvect=linspace(zmid-zfactor*(zend-zstart)/2,zmid+zfactor*(zend-
zstart)/2,references); %Reference vector
yrefvect=.381*ones(1,references);           % Reference vector
z_rcs=linspace(0,3.2004,rcs_z);             % Reconstruction vector
zs=linspace(zstart,zend,Numsources);        % Source vector in z
ys=.381*ones(size(zs));                     % Source vector in y
coherence_criterion=.999;                   % Minimum acceptable
coherence
dB=81;                                      % SNR. If dB>80, no noise
added

Ls_crit=.5;                                 % Coherence length
definition
sigma=1;                                    % Constant in exponential
peak_z=.75;                                 % Center of Gaussian
(number between 0 and 1)
midpoint=(zend-zstart)*peak_z+zstart;       % Calc. cetner of Guassian
source distribution
if lin==1
    q=ones(size(zs));
else
    q=exp(-(zs-midpoint).^2/2/sigma^2);
end
figure                                  % Plot source amplitude vs
position
plot(zs,q)
switch pc
    case 0
        condition='FullyCorrelated';
        part_corr_multiplier=0;
    case 1
        condition='Partiallycorrelated';
        part_corr_multiplier=.7;
    case 2
        condition='Uncorrelated';
    case 3
        condition='Partiallycorrelated_Highcorrelation';
        part_corr_multiplier=.23;
end
cm=[num2str(floor(x_meas*100)),'_',num2str(mod(x_meas*100,1)*10)];
%String format of x_meas
k=2*pi*fint/c;                              % Wave number
```

```
%%% Measurement signals
source_freq=zeros(Numsources,blocks,scans);
source_freq(1,:,:)=randn(1,blocks,scans).*exp(1i*(rand(1,blocks,scans)-
.5)); % Initialize complex amplitudes

% Add specified degree of correlation to the complex amplitudes
% across all sources, scans, and blocks
if abs(pc-2)>0
    source_freq_pc=source_freq;
    for i=2:Numsources
        b=source_freq(1,:,:);
        rand('state',3);
        randn('state',3);
        for l=2:i
            b=(b+part_corr_multiplier*(randn(size(b)).*exp(1i*2*pi*...
(rand(size(b))-.5))));
        end
        source_freq_pc(i,:,:)=b;
    end
else
    rand('state',0);
    for i=1:Numsources
        for h=1:scans
            for l=1:blocks
                temp=randn(1,1).*exp(1i*(rand(1,1)-.5));
                source_freq_pc(i,l,h)=temp;
            end
        end
    end
end
% Apply source amplitude variation
for h=1:scans
    for l=1:blocks
        source_freq_pc(:,l,h)=source_freq_pc(:,l,h).*q.';
    end
end
% Calculate coherence between all the sources
for i=1:Numsources
    for h=1:scans
        temp1=source_freq_pc(:,:,h)*source_freq_pc(:,:,h)'/blocks;
        Css(:,:,h)=temp1;
    end
end
for i=1:Numsources
    for l=1:Numsources
        for h=1:scans

source_coh(i,l,h)=abs(Css(i,l,h)'*Css(i,l,h))^2/abs(Css(i,i,h)'*...
Css(i,i,h))/abs(Css(l,l,h)'*Css(l,l,h));
        end
    end
end
clear temp


% Plot coherence between sources
```

```
figure
source_coh_temp=mean(source_coh,3);
plot(zs-zstart,source_coh_temp(:,:),'-o')
ylabel('Coherence')
xlabel('Meters downstream')
legend('show')
ylim([0 1])

% Determine the coherence lengths according to the sources
for i=1:Numsources
    m=find(source_coh_temp(i:end,i)<Ls_crit,1);


    pol=polyfit(zs(i+m-2:i+m-1),source_coh_temp(i+m-2:i+m-1,i).',1);
    if pol==[0 0]
        Ls(i)=zend;
    else
        Ls(i)=(Ls_crit-pol(2))/pol(1)-zs(i);
    end

end

z_total_scan=linspace(z_scan_start,z_scan_end,meas_z*scans); %Total
scan array in z

% Break up total scan array in z into matrix with rows for the
different
% scans
z_meas=zeros(scans,meas_z);
ind=1;
for i=1:scans
    z_meas(i,:)=z_total_scan(ind:ind+meas_z-1);
    ind=ind+meas_z;
end


%% Get the positions and mag/phase of Sources for blocks and scans
Source=zeros(Numsources*scans*blocks,5);
ind=1;



for h=1:scans
    for l=1:blocks
        for i=1:Numsources
            Source(ind,:)=[0 ys(i) zs(i) abs(source_freq_pc(i,l,h))...
 angle(source_freq_pc(i,l,h))];
            ind=ind+1;
        end
    end
end

r0=Source(:,1:3);   %Matrix of source locations
A=Source(:,4);      %Source magnitudes
```

```
theta=Source(:,5);  %Source phases



%% Set up coordinate grids
Zm=zeros([size(meshgrid(y_meas,z_meas(1,:),x_meas)) scans]);
for i=1:scans
    [Ym,Zm(:,:,i),Xm]=meshgrid(y_meas,z_meas(i,:),x_meas);
end
[Yr,Zr]=meshgrid(y_rcs,z_rcs);
Xr=x_rcs*ones(size(Yr));




%% Calculate complex pressures at reference microphones locations.
%Size=blocks x Number of references x scans
prsq=zeros(blocks,references,scans);
for h=1:scans
    for l=1:blocks
        for i=1:Numsources
            ind=(h-1)*(blocks*Numsources)+(l-1)*Numsources+i;
            prsq(l,:,h)=prsq(l,:,h)+point(x_ref,yrefvect(refvect),...
zrefvect(refvect),r0(ind,:),A(ind),theta(ind),k);
        end
    end
end
%% Calculate coherence at the reference microphones
Crrc=zeros(references,references,scans);
for i=1:references
    for h=1:scans
        temp1=prsq(:,:,h)'*prsq(:,:,h)/blocks;
        Crrc(:,:,h)=temp1;
    end
end
ref_coh=zeros(size(Crrc));

for i=1:references
    for l=1:references
        for h=1:scans

ref_coh(i,l,h)=abs(Crrc(i,l,h)'*Crrc(i,l,h))^2/abs(Crrc(i,i,h)'*...
Crrc(i,i,h))/abs(Crrc(l,l,h)'*Crrc(l,l,h));
        end
    end
end
ref_coh_temp=mean(ref_coh,3);
%% Calculate the coherence lengths according to the reference
%% microphones
Lsr=zeros(size(zrefvect));
for i=1:references
    m=find(ref_coh_temp(i:end,i)<Ls_crit,1);
    pol=polyfit(zrefvect(i+m-2:i+m-1),ref_coh_temp(i+m-2:i+m-1,i).',1);
    if pol==[0 0]
```

```
        Lsr(i)=zrefvect(end);
    else
        Lsr(i)=(Ls_crit-pol(2))/pol(1)-zrefvect(i);
    end
    sloper=mean(diff(Lsr(1:max(find(Lsr<zrefvect(end))))))/...
mean(diff(zrefvect));
    b=Lsr(1)-sloper*zrefvect(1);
    y2=sloper*zrefvect(end)+b;
    slope_funr=sloper*linspace(zrefvect(1),zrefvect(end),references)+b;
end

%% Measured complex pressures
phsq=zeros(length(y_meas),meas_z*scans,blocks);
ind=1;
p_total_sq=zeros(rcs_y,rcs_z,blocks*scans);

% Initialize "measured" and "benchmark" pressures
for h=1:scans
    for l=1:blocks
        for i=1:Numsources
            ind2=(h-1)*(blocks*Numsources)+(l-1)*Numsources+i;
            ind4=(h-1)*(blocks)+l;
            phsq(:,ind:ind+length(z_meas(1,:))-...
1,l)=phsq(:,ind:ind+length(z_meas(1,:))-1,l)+...

point(Xm.',Ym.',Zm(:,:,h).',r0(ind2,:),A(ind2),theta(ind2),k);

p_total_sq(:,:,ind4)=p_total_sq(:,:,ind4)+point(Xr.',Yr.',Zr.',...
r0(ind2,:),A(ind2),theta(ind2),k);
        end
    end
    ind=ind+length(z_meas(1,:));
end
%% Adding noise
rand('state',0);
if dB<=80
    factor1=10^(-dB/20);
    prsqn=prsq;

prsq=prsq+sqrt(mean(mean(mean(prsq))))*factor1*(rand(size(prsq))+1i*...
rand(size(prsq)));

phsq=phsq+sqrt(mean(mean(mean(phsq))))*factor1*(rand(size(phsq))+1i*...
rand(size(phsq)));
else
    prsqn=prsq;

end
p_benchmark=p_total_sq;
p_total_sq=sqrt(sum(abs(p_total_sq).^2/...
max(length(p_total_sq(1,1,:))),3));
%% Plotting and benchmarking
minbench=min(min(min(20*log10(abs(p_total_sq)))));
maxbench=max(max(max(20*log10(abs(p_total_sq)))));

%%%Plot measured pressure over all scans
```

```
[ny,nz]=size(phsq(:,:,1));
yplot=linspace(min(y_meas),max(y_meas),ny);
zplot=linspace(min(min(z_meas)),max(max(z_meas)),nz);
[Y,Z]=meshgrid(yplot,zplot);
%%
pcolor(Z.',Y.',20*log10(mean(abs(phsq),3)))
caxis([minbench maxbench])
axis image
shading interp
xlabel('Z (meters)')
ylabel('Y (meters)')
title({'Meas. pressure averaged over blocks';[num2str(fint),' Hz ',...
 num2str(x_meas*100) ' cm'];[condition]})
%%
figure
pcolor(Zr.',Yr.',20*log10(abs(p_total_sq)))

xlabel('Z (meters)')
ylabel('Y (meters)')
shading interp
axis image
title({'Benchmark (sum of partial fields)';[num2str(fint),' Hz ',...
 num2str(x_rcs*100) ' cm'];[condition, '-- Numerical']})
% caxis([min(minbench,minrcs) max(maxbench,maxrcs)])
colorbar

% Calculate average source amplitude to compare with ref amplitude
source_avg_amp=zeros(1,Numsources);
for i=1:Numsources
    source_avg_amp(i)=norm(A(i:Numsources:end));
end
%%%Stem plot the pressure as measured by the reference microphones
%%%average
figure
avg_r=sqrt(sum(sqrt(sum(abs(prsq).^2,1)/length(prsq(:,1,1))),3)/...
length(prsq(1,1,:)));
% subplot(2,1,1)
stem(zrefvect(refvect),avg_r)

hold on
if references==Numsources
    stem(z_ref,source_avg_amp,'r')
    subplot(2,1,2)
    stem(z_ref,avg_r./source_avg_amp,'g')
    hold on
    stem(z_ref,mean(mean(abs(prsq),1),3))
    [B,IX]=sort(source_avg_amp);
    [B1,IX1]=sort(avg_r);
    amplitudes_right=IX-IX1;
end
xlabel('Z (meters)')
ylabel('Pressure (Pa)')
title('Reference microphone pressure.  Averaged over blocks and scans')
%% Start Virtual Coherence
r_avg=sqrt(sum(abs(prsq).^2,3)/length(prsq(1,1,:)));
%Pack 3-D pressure matrix (y by z by blocks) into 2-D pressure matrix
```

```
%(blocks by y*z)
scan_size=meas_y*meas_z;
p=zeros(blocks,scan_size*scans);
ind=1;
for h=1:meas_z*scans
    for i=1:meas_y
        for l=1:blocks
            p(l,ind)=phsq(i,h,l);
        end
        ind=ind+1;
    end
end
% Initialize virtual coherence variables
Crp=zeros([references meas_y*meas_z scans]);
Crr_sc=zeros(size(r_avg'*r_avg));
U_sc=zeros([size(Crr_sc) scans]);
sigma_sc=zeros(references,1,scans);
V_sc=U_sc;
Sigma_sc=U_sc;
Cvp=Crp;
Crr_scn=Crr_sc;
U_scn=U_sc;
V_scn=V_sc;
sigma_scn=sigma_sc;
%% Compute Crr for each scan as well as Crp and Cpp and Cvp and perform
SVD on each
%% Crr scan
for i=1:scans
    Crr_sc(:,:,i)=prsq(:,:,i)'*prsq(:,:,i)/blocks;
    Crr_scn(:,:,i)=prsqn(:,:,i)'*prsqn(:,:,i)/blocks;
    Crp(:,:,i)=prsq(:,:,i)'*(p(:,(i-
1)*scan_size+1:i*scan_size))/blocks;
    %     Cpp(:,:,i)=p(:,(i-1)*scan_size+1:i*scan_size)'*p(:,(i-
1)*scan_size+1:
    %     i*scan_size)/blocks;  Use this form if scans are more than
    %     one mic each
    [U_sc(:,:,i) sigma_sc(:,:,i) V_sc(:,:,i)]=csvd(Crr_sc(:,:,i));
    [U_scn(:,:,i) sigma_scn(:,:,i) V_scn(:,:,i)]=csvd(Crr_scn(:,:,i));
    Sigma_sc(:,:,i)=diag(sigma_sc(:,:,i));
    Cvp(:,:,i)=U_sc(:,:,i)'*Crp(:,:,i);
end
Cpp(:,:)=p'*p/blocks;
cvv=sigma_sc;
Cvv=Sigma_sc;

%%%Perform Singular Value Decomposition (SVD) on averaged Crr
Crr_a=mean(Crr_sc,3);
[U_a,sigma_a,V_a]=csvd(Crr_a);
Sigma_a=diag(sigma_a);
gamma_2=zeros(meas_y,meas_z*scans,references);
ind=1;
%% Compute virtual coherence function (measured pressure grid size by
number of
%% reference microphones
indpp=1;
for h=1:meas_z*scans
    for i=1:meas_y
```

```
        for l=1:references
            indsc=ceil(h/meas_z);
            factor2=mod(h,meas_z);
            if factor2==0
                factor2=meas_z;
            end
            ind=(factor2-1)*meas_y+i;

gamma_2(i,h,l)=abs(Cvp(l,ind,indsc))^2/Cvv(l,l,indsc)/Cpp(indpp,indpp);
        end
        indpp=indpp+1;
    end
end

%% Use coherence_criterion for each scan to see how many partial fields
are
%% needed and where to truncate the SVD
J=zeros(1,1);
error=zeros(scans,1);
for i=1:scans
    for l=1:references
        ind=meas_z*(i-1)+1;
        temp_sum=sum(gamma_2(:,ind:ind+meas_z-1,1:l),3);
        bool=temp_sum>=coherence_criterion;
        if bool==1
            J(i)=l;
            break
        end
        J(i)=l;
    end
    error(i)=norm(full(spdiags(zeros(J(i),1),0,U_scn(:,1:J(i),i)'*...
U_sc(:,1:J(i),i))))/norm(diag(U_scn(:,1:J(i),i)'*...
U_sc(:,1:J(i),i)))*100;
end

%% Sum of coherence function across all the necessary partial fields
gamma_total=zeros(meas_y,meas_z*scans);
gamma_totaltest=gamma_total;
for i=1:scans
    ind=meas_z*(i-1)+1;
    gamma_total(1:meas_y,ind:ind+meas_z-...
1)=sum(gamma_2(:,ind:ind+meas_z-1,1:J(i)),3);
end

%% Truncate SVD
sigma_michael=sigma_sc;
sigma_sc_inv=zeros(size(sigma_sc));
Sigma_sc_inv=zeros(size(Crr_sc));
Sigma_sc=Sigma_sc_inv;
for i=1:scans
    sigma_sc(J(i)+1:end,:,i)=0;
    sigma_sc_inv(1:J(i),:,i)=1./sigma_sc(1:J(i),:,i);
    Sigma_sc_inv(:,:,i)=diag(sigma_sc_inv(:,:,i));
    Sigma_sc(:,:,i)=diag(sigma_sc(:,:,i));
end
```

```
%% Calculate partial fields (P_hat)
P_hat=zeros(scan_size*scans,references);

for i=1:scans
    P_hat((i-...
1)*scan_size+1:i*scan_size,:)=(U_sc(:,:,i)*(Sigma_sc_inv(:,:,i))*...
U_sc(:,:,i)'*Crp(:,:,i)).'*conj(U_a)*sqrt(Sigma_a);
    %         P_hat((i-
1)*scan_size+1:i*scan_size,:)=(Crp(:,:,i)).'*U_a.'*diag(
    %         sigma_a.^(-1/2)); Use this form if source level variation
is not
    %         needed and better noise averaging is desired

end

%% Unpack P_hat into a 3-D pf for plotting partial fields
pf=zeros([size(phsq(:,:,1).') length(P_hat(1,:))]);
pf2=zeros([size(phsq(:,:,1)) length(P_hat(1,:))]);

for l=1:references
    ind=1;
    for h=1:meas_z*scans
        for i=1:length(y_meas)
            pf2(i,h,l)=P_hat(ind,l);
            %             pf2(i,h,l)=P2hat(ind,l);
            ind=ind+1;
        end
    end
    pf(:,:,l)=pf2(:,:,l).';
end

%% Plotting
figure
mesh(Z.',Y.',real(gamma_total))

title('Coherence at measured points')
shading interp
colorbar
zlim([0 1])
view([-5 22])


%%%Plot the singular values of averaged Crr
if references>1
    figure
    sa=diag(Sigma_a);
    plot(10*log10(sa),'o')
    title('Singular Values of Crr averaged over scans')
    ylabel('10log_{10}')
    colorbar
end

% Plot ref locations vs. source locations
figure
scatter(zs,ys,'o','linewidth',3,'sizedata',300)
```

```
hold on
scatter(zrefvect(refvect),yrefvect(refvect),'r+','linewidth',...
3,'sizedata',300)
ylim([min(y_meas) max(y_meas)])
xlim([z_scan_start z_scan_end])
xlabel('Z (meters)')
ylabel('Y (meters)')
legend('Source','Ref mic')
title('Locations')

% Only use a the median of J (across scans) partial fields
pf=pf(:,:,1:median(J));
%     pf2=pf2(:,:,1:max(J));

figure
bool=1;
% Plot partial fields (up to 12)
m=min(median(J),12);

for i=1:m
    if floor(median((J)))>3
        while bool
            fact=factor(m);
            if isscalar(fact)
                m=m+1;
            else
                bool=0;
            end
        end
        if length(fact)<3
            subplot(fact(2),fact(1),i)
        else
            subplot(prod(fact(3:end)),prod(fact(1:2)),i)
        end
    else
        subplot(median(J),1,i);
    end

    pcolor(Z,Y,20*log10(abs(pf(:,:,i))))
    shading interp
    colorbar
    daspect([1 1 1])
    title(['#',num2str(i)])

end

%% Send the partial fields to SONAH and calculate the final magnitude
of P

pf_total=0;
% Sum partial fields
for i=1:median(J)
    pf_total=pf_total+abs(pf(:,:,i)).^2;
end
pf_total=sqrt(pf_total);
```

```
figure
% subplot(2,2,3)
pcolor(Z,Y,20*log10(pf_total))
axis image
shading interp
% caxis([minbench maxbench])
% colormap(gray)
colorbar
xlabel('Z (meters)')
ylabel('Y (meters)')
title({['Sum of partial fields (',...
num2str(floor(mean((J)))),')'];...
[num2str(fint),' Hz ', num2str(x_meas*100) ...
 ' cm'];[condition, '-- Numerical']})
%% SONAH

[P,Ux,Uy,Uz]=sonah(Z,Y,Zr,Yr,x_meas,pf,x_rcs,fint);
clear global U1 V1 G1

%% Sum reconstructed partial fields
P_total=0;
for i=1:length(P(1,1,:))
    P_total=P_total+abs(P(:,:,i).^2);
    %     P2_total=P2_total+abs(P2(:,:,i).^2);
end
figure
bool=1;
m=min(median(J),12);
% Plot reconstructed partial fields
for i=1:m
    if median(J)>3
        while bool
            fact=factor(m);
            if isscalar(fact)
                m=m+1;
            else
                bool=0;
            end
        end
        if length(fact)<3
            subplot(fact(2),fact(1),i)
        else
            subplot(prod(fact(3:end)),prod(fact(1:2)),i)
        end
    else
        subplot(median(J),1,i);
    end
    pcolor(Zr,Yr,20*log10(abs(P(:,:,i))))
    shading interp
    colorbar
    daspect([1 1 1])
    title(['Rcs #',num2str(i)])
end

P_total=sqrt(P_total);
% Calculate limits for plot comparisons
```

```
minbench=20*log10(min(min(min(abs(p_total_sq)))));
maxbench=20*log10(max(max(max(abs(p_total_sq)))));
minrcs=20*log10(min(min(min(abs(P_total)))));
maxrcs=20*log10(max(max(max(abs(P_total)))));

%% Plotting results
% Plot benchmark
figure
pcolor(Zr.',Yr.',20*log10(abs(p_total_sq)))

xlabel('Z (meters)')
ylabel('Y (meters)')
shading interp
axis image
title({'Benchmark (sum of partial fields)';[num2str(fint),' Hz ',
num2str(x_rcs*100) ' cm'];[condition, '-- Numerical']})
caxis([min(minbench,minrcs) max(maxbench,maxrcs)])
colorbar

% Calculate Error
dBerr=(20*log10(abs(P_total.')./abs(p_total_sq)));
meanerror=sqrt(mean(mean(dBerr.^2)));
stderror=std(std(dBerr));
percent_error=sqrt(sum(sum(abs(P_total.'-
p_total_sq).^2))/sum(sum(abs(p_total_sq).^2)))*100;

% Plot the centerline SPL for benchmark, reconstruction, and sum of
% partial fields
figure
plot(z_rcs,20*log10(P_total(:,floor(median(1:min(size(P_total))))))/...
20e-6))
hold on
plot(z_rcs,...
20*log10(p_total_sq(floor(median(1:min(size(p_total_sq)))),:)/...
20e-6),'r--')
hold on
plot(z_total_scan,20*log10(max(pf_total.')),'g:')
xlabel('Z meters')
ylabel('dB')
legend('Reconstructed','Benchmark','Partial field
sum','location','best')
title(['Comparison @ y = 0 for ', num2str(fint), 'Hz and ',
num2str(x_rcs*100), ' cm'])

% Plot dB error
% figure
% pcolor(Zr.',Yr.',dBerr)
% axis image
% shading interp
% colorbar
% title(['dB error ', num2str(meanerror)])
% xlabel('Z (meters)')
% ylabel('Y (meters)')

%  Calculate and plot intensity
ix=zeros(size(P));
```

```
iy=ix;
iz=ix;


ix=1/2*real(P.*conj(Ux));
iy=1/2*real(P.*conj(Uy));
iz=1/2*real(P.*conj(Uz));

figure
surf(x_rcs*ones(size(Yr)),Yr,Zr,20*log10(abs(P_total)/20e-6))
hold on
shading interp
% axis image
% zlim([-.1 3.3])
% xlim([-.3 .5])
% ylim([-.1 2])
axis image
h=colorbar;
title(h,'SPL')
view([-35 45])
quiver3(x_rcs*ones(size(Yr)),Yr,Zr,sum(ix,3),sum(iy,3),sum(iz,3),2,...
'w','linewidth',2,'maxheadsize',4)
% title('Reconstructed SPL and Intensity--900 Hz')
xlabel('X (meters)')
ylabel('Y (meters)')
zlabel('Z (meters)')


% Calculate references per coherence length plot and print rplc and
print
% errors, reference SPL range, and mean virtual coherence
refs_per_Ls=
mean(Lsr(1:max(find(Lsr<zrefvect(end))))/mean(diff(zrefvect));
figure
plot(zrefvect,Lsr,'r')
title(['Coherence Lengths versus position ', num2str(refs_per_Ls),...
' mics per coherence length'])
xlabel('Z (meters)')
ylabel('Coherence length (meters)')
avg_r_spl=20*log10(avg_r/20e-6);
r_range=max(avg_r_spl)-min(avg_r_spl);
mean_vc=mean(mean(gamma_total));
```

SONAH sub-function

```
function [pmapped, Ux, Uy, Uz]=sonah(Z,Y,Zr,Yr,x_meas,pf,x_rcs,f)
global U G V A alpha betax betay betaz
```

```
factor=.001;
sz=size(pf);
if length(sz)<3
    sz(3)=1;
end
for ii=1:sz(3)
    xh=x_meas;          % hologram radius
    xr=x_rcs;           % reconstruction radius
    c=343;              % Speed of sound
    k=2*pi*f/c;         % Wave number
    omega=k*c;          % Angular frequency
    rho0=1.21;          % Density


    % Convert 2-d position matrices to position vectors
    z=Z(:,1);
    y=Y(1,:);
    zr=Zr(:,1);
    yr=Yr(1,:);
    Xr=xr*ones(size(Yr));

    % Convert 2-d pressure matrix into 1-d array
    p=reshape(pf(:,:,ii),1,length(z)*length(y));
    % Determine maximum k values to use in the wave function matrices
    kzmax=2*pi/mean(diff(z));
    kymax=2*pi/mean(diff(y));
    % Determine delta ky and delta kz
    dky=pi/(y(end)-y(1))/2;
    dkz=pi/(z(end)-z(1))/2;
    kz=-kzmax:dkz:kzmax;
    ky=-kymax:dky:kymax;
    % Don't let number of wave functions in each direction go above 800
    % memory issues
    if length(kz)>800
        kz=linspace(-kzmax,kzmax,800);
    end
    if length(ky)>800
        ky=linspace(-kymax,kymax,800);
    end

    % Make use of global variables to reduce variable loading time
    % while maximizing available memory (continuing to clear each loop)
    if isempty(A)
        A=zeros(length(ky)*length(kz),length(y)*length(z));


        %Construct A matrix values of wave functions at the measurement
positions
        cc=1;
        rr=1;
        F0=1;
        for i=1:length(y)
            for h=1:length(z)
                for n=1:length(kz)
                    A(cc:cc+length(ky)-1,rr)=F0*sqrt(k./...
abs(sqrt(k^2-(kz(n)^2+ky.^2)))).*...
```

```
exp(-j*(kz(n)*z(h)+ky*y(i)+conj(sqrt(k^2-...
(kz(n)^2+ky.^2)))*(xh)));
                    cc=cc+length(ky);
                end
                cc=1;
                rr=rr+1;
            end
        end
        alpha=zeros(length(ky)*length(kz),length(yr)*length(zr));
        betax=alpha;
        betay=alpha;
        betaz=alpha;
        cc=1;
        rr=1;
        % Construct alpha ,betax,betay, and betaz matrices
        % (for pressure,Ux,Uy, and Uz, respectively
        for i=1:length(yr)
            for h=1:length(zr)
                for n=1:length(kz)
                    alpha(cc:cc+length(ky)-...
1,rr)=F0*sqrt(k./abs(sqrt(k^2-...
(kz(n)^2+ky.^2)))).*exp(-j*(kz(n)*zr(h)+ky*yr(i)+conj(sqrt(k^2-...
(kz(n)^2+ky.^2)))*(xr)));

                    betax(cc:cc+length(ky)-...
1,rr)=F0*sqrt(k./abs(sqrt(k^2-...
(kz(n)^2+ky.^2)))).*conj(sqrt(k^2-(kz(n)^2+ky.^2)))/omega/rho0.*exp(-
...
j*(kz(n)*zr(h)+ky*yr(i)+conj(sqrt(k^2-(kz(n)^2+ky.^2)))*(xr)));
                    betay(cc:cc+length(ky)-...
1,rr)=F0*sqrt(k./abs(sqrt(k^2-...
(kz(n)^2+ky.^2)))).*ky/omega/rho0.*exp(-...
j*(kz(n)*zr(h)+ky*yr(i)+conj(sqrt(k^2-(kz(n)^2+ky.^2)))*(xr)));
                    betaz(cc:cc+length(ky)-...
1,rr)=F0*sqrt(k./abs(sqrt(k^2-...
(kz(n)^2+ky.^2))))*kz(n)/omega/rho0.*exp(-...
j*(kz(n)*zr(h)+ky*yr(i)+conj(sqrt(k^2-(kz(n)^2+ky.^2)))*(xr)));
                    cc=cc+length(ky);
                end
                cc=1;
                rr=rr+1;
            end
        end
    end
end
%% Commence regularization (modified Tikhonov)
if isempty(U)
    [U,G,V]=csvd(A'*A);
end
%% Begine autmoatic process to find regularization parameter alpha via
%% modified generalized cross-validation
reg_alpha=logspace(-25,5,100);
J=zeros(1,length(reg_alpha));
for n=1:length(reg_alpha)
    J(n)=modgcvfun(reg_alpha(n),G,V,p.');
end
```

```
[low,ind]=min(J);
alphalow=reg_alpha(ind);

reg_alpha=fminbnd('modgcvfun',.01*alphalow,100*alphalow,...
optimset('Display','off'),G,V,p.');

g=diag(G);

% Determine the regularized inverse of A'*A
F1alpha=diag(reg_alpha./(reg_alpha+G.^2));
Ralpha=V*(reg_alpha*F1alpha.^2+g'*g)^(-1)*g'*U';

% Calculate reconstructed acoustic quantities
p1=p*Ralpha*A'*alpha;
ux=p*Ralpha*A'*betax;
uy=p*Ralpha*A'*betay;
uz=p*Ralpha*A'*betaz;
ind=1;

% Reload 1-d reconstructions into 2-d matrices for plotting
if ii==1
    pmapped=zeros(length(zr),length(yr),sz(3));
    Ux=pmapped;
    Uy=pmapped;
    Uz=pmapped;
end
pmapped(:,:,ii)=reshape(p1,length(zr),length(yr));
Ux(:,:,ii)=reshape(ux,length(zr),length(yr));
Uy(:,:,ii)=reshape(uy,length(zr),length(yr));
Uz(:,:,ii)=reshape(uz,length(zr),length(yr));

end
```

CSVD sub-function

```
function [U,s,V] = csvd(A,tst)
%CSVD Compact singular value decomposition.
%
% s = csvd(A)
% [U,s,V] = csvd(A)
% [U,s,V] = csvd(A,'full')
%
% Computes the compact form of the SVD of A:
%    A = U*diag(s)*V',
% where
%    U  is  m-by-min(m,n)
%    s  is  min(m,n)-by-1
```

```
%    V  is  n-by-min(m,n).
%
% If a second argument is present, the full U and V are returned.

% Per Christian Hansen, IMM, 06/22/93.

if (nargin==1)
    if (nargout > 1)
        [m,n] = size(A);
        if (m >= n)
            [U,s,V] = svd(full(A),0); s = diag(s);
        else
            [V,s,U] = svd(full(A)',0); s = diag(s);
        end
    else
        U = svd(full(A));
    end
else
    if (nargout > 1)
        [U,s,V] = svd(full(A)); s = diag(s);
    else
        U = svd(full(A));
    end
end
```

MODGCVFUN sub-function

```
function J=modgcvfun(alpha,s1,U1,ph)

    F1alpha1=diag(alpha./(alpha+s1.^2.*((alpha+s1.^2)/alpha).^2));
    J=norm(F1alpha1*U1'*ph)^2/trace(F1alpha1)^2;
```

POINT sub-funtion

```
function p=point(X,Y,Z,r0,A,theta,k);

dist=sqrt((X-r0(1)).^2+(Y-r0(2)).^2+(Z-r0(3)).^2);
p=A./dist.*exp(-j*k*dist)*exp(j*theta);
```